



CERN-PH-EP/2013-037

2015/09/07

CMS-HIG-14-004

Search for the standard model Higgs boson produced through vector boson fusion and decaying to $b\bar{b}$

The CMS Collaboration^{*}

Abstract

A first search is reported for a standard model Higgs boson (H) that is produced through vector boson fusion and decays to a bottom-quark pair. Two data samples, corresponding to integrated luminosities of 19.8 fb^{-1} and 18.3 fb^{-1} of proton-proton collisions at $\sqrt{s} = 8 \text{ TeV}$ were selected for this channel at the CERN LHC. The observed significance in these data samples for a $H \rightarrow b\bar{b}$ signal at a mass of 125 GeV is 2.2 standard deviations, while the expected significance is 0.8 standard deviations. The fitted signal strength $\mu = \sigma/\sigma_{\text{SM}} = 2.8^{+1.6}_{-1.4}$. The combination of this result with other CMS searches for the Higgs boson decaying to a b -quark pair, yields a signal strength of 1.0 ± 0.4 , corresponding to a signal significance of 2.6 standard deviations for a Higgs boson mass of 125 GeV .

Published in Physical Review D as doi:10.1103/PhysRevD.92.032008.

1 Introduction

In the standard model (SM) [1–3], the electroweak symmetry breaking is achieved by a mechanism [4–6] that provides mass to the electroweak gauge bosons, while leaving the photon massless. The mechanism predicts the existence of a scalar Higgs boson (H), and its observation was one of the main goals of the CERN LHC program. A boson with mass near 125 GeV was recently discovered by both the ATLAS [7] and CMS [8, 9] collaborations, with properties that are compatible with those of a SM Higgs boson [10, 11].

At the LHC, a SM Higgs boson can be produced through a variety of mechanisms. The expected production cross sections [12] as a function of the Higgs boson mass are such that, in the mass range considered in this study, the vector boson fusion (VBF) process $pp \rightarrow qqH$ has the second largest production cross section following gluon fusion (GF). Furthermore, for a SM Higgs boson with a mass $m_H \lesssim 135$ GeV, the expected dominant decay mode is to a b-quark pair (bb).

Thus far, the search for $H \rightarrow bb\bar{b}$ has been carried out in the associated production process involving a W or a Z boson (VH production) at the Tevatron [13] and at the LHC [14, 15], as well as in association with a top quark pair at the LHC [16–18], without reaching the necessary sensitivity to observe the Higgs boson in this decay channel. It is therefore important to exploit other production modes, such as VBF, to provide in the $bb\bar{b}$ decay channel further information on the nature and properties of the Higgs boson.

The prominent feature of the VBF process $qqH \rightarrow qqbb\bar{b}$ is the presence of four energetic jets in the final state. Two jets are expected to originate from a light-quark pair (u or d), which are typically two valence quarks from each of the colliding protons scattered away from the beam line in the VBF process. These “VBF-tagging” jets are expected to be roughly in the forward and backward directions relative to the beam direction. Two additional jets are expected from the Higgs boson decay to a $bb\bar{b}$ pair in more central regions of the detector. Another important property of the signal events is that, being produced through an electroweak process, no quantum chromodynamics (QCD) color is exchanged at leading order in the production. As a result, in the most probable color evolution of these events, the VBF-tagging jets connect to the proton remnants in the forward and backward beam line directions, while the two b-quark jets connect to each other as decay products of the color neutral Higgs boson. Consequently very little additional QCD radiation and hadronic activity is expected in the space outside the color-connected regions, in particular in the whole rapidity interval (rapidity gap) between the two VBF-tagging jets, with the exception of the Higgs boson decay products.

The dominant background to this search is from QCD production of multijet events. Other backgrounds arise from: (i) hadronic decays of Z or W bosons produced in association with additional jets, (ii) hadronic decays of top quark pairs, and (iii) hadronic decays of singly produced top quarks. The contribution of the Higgs boson in GF processes with two or more associated jets is included in the expected signal yield.

The search is performed on selected four-jet events that are characterized by the response of a multivariate discriminant trained to separate signal events from background without making use of kinematic information on the two b-jet candidates. Subsequently, the invariant mass distribution of two b jets is analyzed in each category in the search for a signal “bump” above the smooth contribution from the SM background. This is the first search of this kind, and the only search for the SM Higgs boson in all-jet final states at the LHC. A search for a SM Higgs boson in the all-hadronic final state has been previously reported by the CDF experiment [19].

This paper is organized as follows: Section 2 highlights the features of the CMS detector needed to perform this analysis. Section 3 details the production of simulated samples used to study

the signal and main backgrounds, and Section 4 presents the employed triggers. Event reconstruction and selection are described in Sections 5 and 6, respectively. The unique features of the analysis are discussed in Section 7, which includes the improvement of the resolution in jet transverse momentum (p_T) by regression techniques, discrimination between quark- and gluon-originated jets, and soft QCD activity. An important validation of the analysis strategy is the observation of the $Z \rightarrow b\bar{b}$ decay, which is presented in Section 8. The search for a SM Higgs boson is discussed in Section 9 and the associated systematic uncertainties are presented in Section 10. The final results are discussed in Section 11 and combined with previous searches in the same channel in Section 12. We summarize in Section 13.

2 The CMS detector

The central feature of the CMS apparatus is a superconducting solenoid of 6 m internal diameter, providing a magnetic field of 3.8 T. A silicon pixel and strip tracker, a lead tungstate crystal electromagnetic calorimeter, and a brass and scintillator hadron calorimeter are located within the solenoidal field. Muons are measured in gas-ionization detectors embedded in the steel flux-return yoke of the solenoid. Forward calorimetry (pseudorapidity $3 < |\eta| < 5$) complements the coverage provided by the barrel ($|\eta| < 1.3$) and end cap ($1.3 < |\eta| < 3$) detectors. The first level (L1) of the CMS trigger system, composed of specialized processors, uses information from the calorimeters and muon detectors to select the most interesting events in a time interval of less than 4 μ s. The high-level trigger (HLT) processor farm decreases the event rate from about 100 kHz to less than 1 kHz, before data storage. A more detailed description of the CMS apparatus and the main kinematic variables used in the analysis can be found in Ref. [20].

3 Simulated samples

Samples of simulated Monte Carlo (MC) signal and background events are used to guide the analysis optimization and to estimate signal yields. Several event generators are used to produce the MC events. The samples of VBF and GF signal processes are generated using the next-to-leading order perturbative QCD program POWHEG 1.0 [21], interfaced to TAUOLA 2.7 [22] and PYTHIA 6.4.26 [23] for the hadronization process and modeling of the underlying event (UE). The most recent PYTHIA 6 Z2* tune is derived from the Z1 tune [24], which uses the CTEQ5L parton distribution functions (PDF), whereas Z2* adopts CTEQ6L [25]. The signal samples are generated using only $H \rightarrow b\bar{b}$ decays, for five mass hypotheses: $m_H = 115, 120, 125, 130$, and 135 GeV .

Background samples of QCD multijet, $Z + \text{jets}$, $W + \text{jets}$, and $t\bar{t}$ events are simulated using leading-order (LO) MADGRAPH 5.1.3.2 [26] interfaced with PYTHIA. The single top quark background samples are produced using POWHEG, interfaced with TAUOLA and PYTHIA. The default set of PDF used with POWHEG samples is CT10 [27], while the LO CTEQ6L1 set [25] is used for other samples. The production cross sections for $W + \text{jets}$ and $Z + \text{jets}$ are rescaled to next-to-next-to-leading-order (NNLO) cross sections calculated using the FEWZ 3.1 program [28–30]. The $t\bar{t}$ and single top quark samples are also rescaled to their cross sections based on NNLO calculations [31, 32].

To accurately simulate the LHC luminosity conditions during data taking, additional simulated pp interactions overlapping in the same or neighboring bunch crossings of the main interaction, denoted as pileup, are added to the simulated events with a multiplicity distribution that matches the one in the data.

4 Triggers

The data used for this analysis were collected using two different trigger strategies that result in two different data samples for analysis. First, a set of dedicated trigger event selection (paths) was specifically designed and deployed for the VBF $q\bar{q}H \rightarrow q\bar{q}b\bar{b}$ signal search, both for the L1 trigger and the HLT, and operated during the full 2012 data taking. Then, a more general trigger was employed for the larger part of the 2012 data taking that targeted VBF signatures in general. The first (nominal) set of triggers collected the larger fraction of the signal events, while the second trigger supplemented the search with events that failed the stringent nominal-trigger requirements. The integrated luminosity collected with the first set of triggers was 19.8 fb^{-1} , while for the second trigger it was 18.3 fb^{-1} .

While the first dedicated trigger paths collected data within the standard CMS streams, the second general-purpose VBF trigger path ran in parallel with data streams that were reconstructed later, in 2013, during the LHC upgrade.

4.1 Dedicated signal trigger

The L1 paths require the presence of at least three jets with p_T above decreasing thresholds $p_T^{(1)}, p_T^{(2)}, p_T^{(3)}$ that were adjusted according to the instantaneous luminosity [$p_T^{(1)} = 64\text{--}68 \text{ GeV}$, $p_T^{(2)} = 44\text{--}48 \text{ GeV}$, $p_T^{(3)} = 24\text{--}32 \text{ GeV}$]. Among the three jets, one and only one of the two leading jets [with $p_T > p_T^{(1)}, p_T^{(2)}$] can be in the forward region with pseudorapidity $2.6 < |\eta| \leq 5.2$, while the other two jets are required to be central ($|\eta| \leq 2.6$).

The HLT paths are seeded by the L1 paths described above, and require the presence of four jets with p_T above thresholds that were again adjusted according to the instantaneous luminosity, $p_T > 75\text{--}82, 55\text{--}65, 35\text{--}48$, and $20\text{--}35 \text{ GeV}$, respectively. Two complementary HLT paths have been employed that make use, respectively, of (i) only calorimeter-based jets (CaloJets) and (ii) particle-flow jets (PFJets, see Section 5). At least one of the four selected jets must further fulfill minimum b-tagging requirements, evaluated using HLT regional tracking around the jets, and using the “track counting high-efficiency” (TCHE) or the “combined secondary vertex” (CSV) algorithms [33], alternatively for the first and second paths. Events are accepted if they satisfy either of the two paths.

Among the four leading jets, the light-quark ($q\bar{q}$) VBF-tagging jet pair is assigned in one of two ways: (i) the pair with the smallest HLT b-tagging output values (b-tag-sorted $q\bar{q}$) or (ii) the pair with the maximum pseudorapidity difference (η -sorted $q\bar{q}$). Both pairs are required to exceed variable minimum thresholds on $|\Delta\eta_{q\bar{q}}|$ of 2.2–2.5, and of $200\text{--}240 \text{ GeV}$ on the dijet invariant mass $m_{q\bar{q}}$, depending on the instantaneous luminosity.

To evaluate trigger efficiencies, a prescaled control path is used, requiring one PFJet with $p_T > 80 \text{ GeV}$. To match the efficiency in data, the simulated trigger efficiency must be corrected with a scale factor of order 0.75 that is parametrized a function of the highest jet b-tag output in the event and the invariant mass of the quark-jet candidates. With this procedure the weak dependence of the trigger efficiencies on the invariant mass of the two b jets is also taken into account.

4.2 General-purpose VBF trigger

The L1 paths for the general-purpose VBF trigger require that the scalar p_T sum of the hadronic activity in the event exceeds 175 or 200 GeV, depending on the instantaneous luminosity.

The HLT path is seeded by the L1 path described above, and requires the presence of at least

two CaloJets with $p_T > 35\text{ GeV}$. Out of all the possible jet pairs in the event, with one jet lying at positive and the other at negative η , the pair with the highest invariant mass is selected as the most probable VBF-tagging jet pair. The corresponding invariant mass m_{jj}^{trig} and absolute pseudorapidity difference $|\Delta\eta_{jj}^{\text{trig}}|$ are required to be larger than 700 GeV and 3.5 , respectively.

The efficiency of the general-purpose VBF trigger is measured in a similar way as for the dedicated triggers, using a prescaled path (requiring two PFJets with average $p_T > 80\text{ GeV}$). To match the efficiency in data, the simulated trigger efficiency must be corrected with a scale factor of order 0.8 that is expressed as a function of the invariant mass and the pseudorapidity difference of the two offline quark-jet candidates.

5 Event reconstruction

The offline analysis uses reconstructed charged-particle tracks and candidates from the particle-flow (PF) algorithm [34–36]. In the PF event reconstruction all stable particles in the event, i.e. electrons, muons, photons, and charged and neutral hadrons, are reconstructed as PF candidates using information from all CMS subdetectors to obtain an optimal determination of their direction, energy, and type. The PF candidates are then used to reconstruct the jets and missing transverse energy.

Jets are reconstructed by clustering PF candidates with the anti- k_T algorithm [37, 38] with a distance parameter of 0.5 . Reconstructed jets require a small additional energy correction, mostly due to thresholds on reconstructed tracks and clusters in the PF algorithm and various reconstruction inefficiencies [39]. Jet identification criteria are also applied to reject misreconstructed jets resulting from detector noise, as well as jets heavily contaminated with pileup energy (clustering of energy deposits not associated with a parton from the primary pp interaction) [40]. The efficiency of the jet identification criteria is greater than 99% , with the rejection of 90% of background pileup jets with $p_T \simeq 50\text{ GeV}$.

The identification of jets that originate from the hadronization of b quarks is done with the CSV b tagger [33], also implemented for the HLT paths, as described in Section 4. The CSV algorithm combines the information from track impact parameters and secondary vertices identified within a given jet, and provides a continuous discriminator output.

Events are required to have at least four reconstructed jets. All the jets found in an event are ordered according to their p_T , and the four leading ones are considered as the most probable b jet and VBF-tagging jet candidates. The distinction between the two jet types is done by the means of a multivariate discriminant that, in addition to the b-tag values and the b-tag ordering, takes into account the η values and the η ordering. In the VBF $H \rightarrow b\bar{b}$ signal simulation it is found that the b jets have higher b-tag values and are more central in η than the VBF-tagging jets. A boosted decision tree (BDT), implemented with the TMVA package [41], is trained on simulated signal events using the discriminating variables previously described and its output is used as a b-jet likelihood score; out of the four leading jets the two with the highest score are identified as the b jets, while the other two are identified as the VBF-tagging jets. With the use of the multivariate b-jet assignment the signal efficiency is increased by $\approx 10\%$ compared to the interpretation based on CSV output only.

6 Event selection

The offline event selection is based upon the b-jet and VBF-tagging jet assignment described in Section 5, and is adjusted to the two different trigger sets presented in Section 4. In what follows the selected events are divided into two sets referred to as *set A* and *set B*. These selections are summarized in Table 1.

Events selected in set A are required to have been selected by the dedicated VBF $\text{qqH} \rightarrow \text{qq}\bar{b}\bar{b}$ trigger and to have at least four PF jets with $p_T^{1,2,3,4} > 80, 70, 50, 40 \text{ GeV}$ and $|\eta| < 4.5$. Moreover, at least two of these jets must satisfy the loose CSV working point requirement (CSVL) [33]. The VBF topology is ensured by requiring $m_{\text{qq}} > 250 \text{ GeV}$ and $|\Delta\eta_{\text{qq}}| > 2.5$, where qq denotes the pair of the most probable VBF-tagging jets. Finally, in order to suppress further the background, the azimuthal angle difference $\Delta\phi_{\text{bb}}$ between the two b-jet candidates must be less than 2.0 radians. Figure 1 shows the normalized distributions of $|\Delta\eta_{\text{qq}}|$ (left) and $\Delta\phi_{\text{bb}}$ (right) for the sum of all simulated backgrounds, and the VBF and GF Higgs boson production.

Events in set B are first required to not belong to set A (to avoid double counting). Then, they must have passed the generic VBF topological trigger and have at least four PF jets with $p_T > 30 \text{ GeV}$ and $|\eta| < 4.5$. In addition, the scalar p_T sum of the two leading jets must be greater than 160 GeV . In order to enrich the sample in b jets, there must be at least one jet satisfying the medium CSV working point requirement (CSVM) [33] and one jet satisfying the CSVL. The VBF topology is ensured by requiring $m_{\text{qq}}, m_{\text{jj}}^{\text{trig}} > 700 \text{ GeV}$, and $|\Delta\eta_{\text{qq}}|, |\Delta\eta_{\text{jj}}^{\text{trig}}| > 3.5$, where qq denotes the pair of the most probable VBF jets and jj denotes the jet pair with the highest invariant mass (as in the trigger logic described in Section 4). Finally the azimuthal angle $\Delta\phi_{\text{bb}}$ between the two b-jet candidates must be less than 2.0 radians.

After all the selection requirements, 2.3% of the simulated VBF signal events (for $m_H = 125 \text{ GeV}$) end up in set A, and 0.8% end up in set B. The fraction of events in set A that also satisfy the requirements of set B (except for the set A veto) amounts to 39%. The set B selection recovers signal events presenting pronounced VBF jets, with lower p_T but larger pseudorapidity opening and invariant mass.

Table 1: Summary of selection requirements for the two analyses.

	Set A	Set B
Trigger	Dedicated VBF $\text{qqH} \rightarrow \text{qq}\bar{b}\bar{b}$	General-purpose VBF trigger $p_T^{1,2,3,4} > 30 \text{ GeV}$
Jets p_T	$p_T^{1,2,3,4} > 80, 70, 50, 40 \text{ GeV}$	$p_T^1 + p_T^2 > 160 \text{ GeV}$
Jets $ \eta $	< 4.5	< 4.5
b tag	At least 2 CSVL jets	At least 1 CSVM and 1 CSVL jets
$\Delta\phi_{\text{bb}}$	$< 2.0 \text{ radians}$	$< 2.0 \text{ radians}$
VBF topology	$m_{\text{qq}} > 250 \text{ GeV}$	$m_{\text{qq}}, m_{\text{jj}}^{\text{trig}} > 700 \text{ GeV}$
	$ \Delta\eta_{\text{qq}} > 2.5$	$ \Delta\eta_{\text{qq}} , \Delta\eta_{\text{jj}}^{\text{trig}} > 3.5$
Veto	None	Events that belong to set A

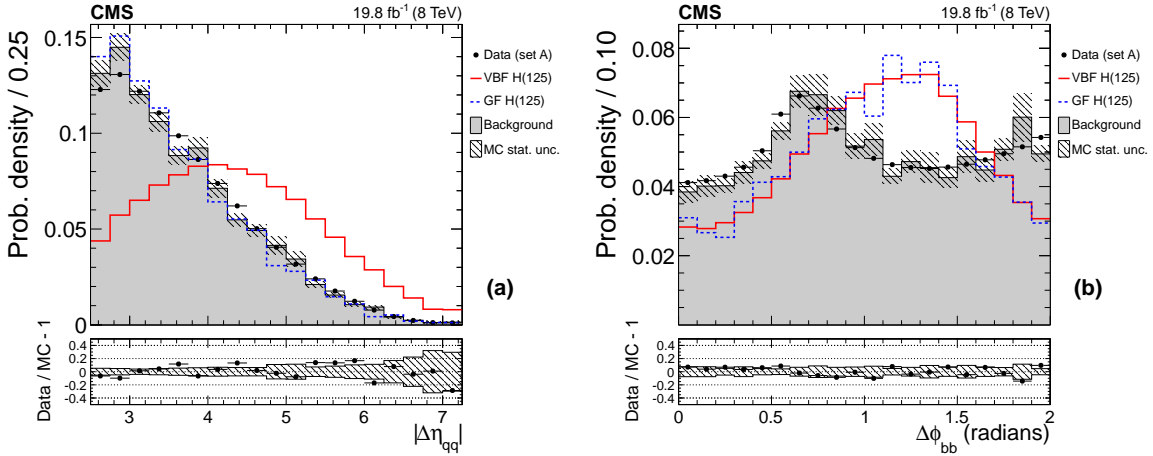


Figure 1: (a) Normalized distribution in absolute pseudorapidity difference between the two VBF-jet candidates ($|\Delta\eta_{qq}|$). (b) Normalized distribution of the azimuthal difference between the two b-jet candidates ($\Delta\phi_{bb}$). The selection corresponds to set A, data are shown by the points, and the sum of all simulated backgrounds is by the filled histograms. The VBF Higgs boson signal is displayed by a solid line, and the GF Higgs boson signal is shown by a dashed line. The panels at the bottom show the fractional difference between data and background simulation, with the shaded band representing the statistical uncertainties in the MC samples.

7 Signal properties

The analysis described in this paper relies on certain characteristic properties of the studied final state, which provide a significant improvement of the overall sensitivity. First, the resolution of the invariant mass of the two b jets is improved by applying multivariate regression techniques. Then, the jet composition properties are used to form a discriminant that separates jets originating from light quarks or gluons. Third, soft QCD activity outside the jets is quantified and used as a discriminant between QCD processes with strong color flow and the VBF signal without color flow.

7.1 Jet transverse-momentum regression

The $b\bar{b}$ mass resolution is improved by using a regression technique similar to those used in the search for a Higgs boson produced in association with a weak vector boson and decaying to $b\bar{b}$ [14]. A refined calibration is carried out for individual b jets, beyond the default jet energy corrections, that takes into account the jet composition properties and targets semileptonic b decays that lead to a substantial mismeasurement of the jet p_T due to the presence of an escaping neutrino. For this purpose a regression BDT is trained on simulated signal events with inputs including information about the jet properties and structure. The target of the regression is the p_T of the associated particle-level jet, clustered from all stable particles (with lifetime $c\tau > 1$ cm). The inputs include: (i) the jet p_T , η , and mass; (ii) the jet energy fractions carried by neutral hadrons and photons [34–36]; (iii) the mass and the uncertainty in the decay length associated with the secondary vertex, when present; (iv) the event missing transverse energy and its azimuthal direction relative to the jet; (v) the total number of jet constituents; (vi) the p_T of the soft-lepton candidate inside the jet, when present, and its p_T component perpendicular to the jet axis; (vii) the p_T of the leading track in the jet; and (viii) the average p_T density of the event in y - ϕ space (FASTJET ρ method [42]).

The additional energy correction of b jets leads to an improvement of the jet p_T resolution, which in turn improves the dijet invariant mass resolution by approximately 17% in the phase

space of the offline event selections. Figure 2 shows the reconstructed dijet invariant mass of the b-jet candidates (m_{bb}) before and after the regression for simulated events passing set A selections. The measured distribution of the regressed m_{bb} in set A is shown in Fig. 3.

The validation of the regression technique in data is done with samples of $Z \rightarrow \ell\ell$ events with one or two b-tagged jets. When the jets are corrected by the regression procedure, the p_T balance distribution, between the Z boson, reconstructed from the leptons, and the b-tagged jet or dijet system is improved to be better centered at zero and narrower than when the regression correction is not applied. In both cases the distributions for data and the simulated samples are in good agreement after the regression correction is applied.

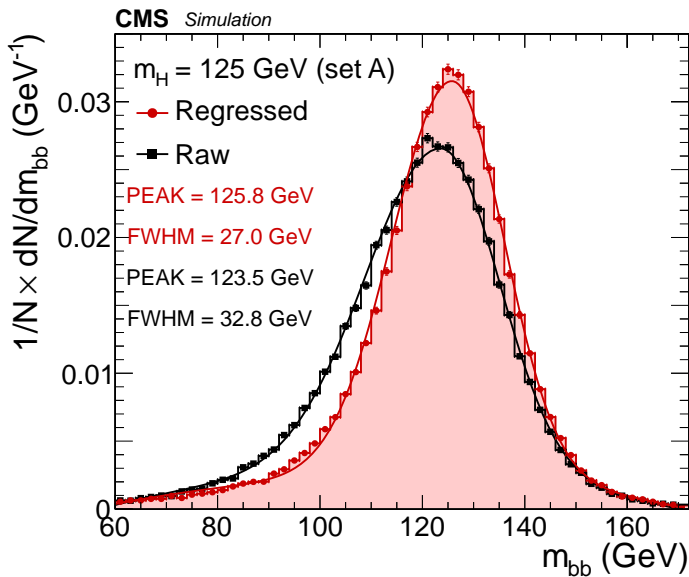


Figure 2: Simulated invariant mass distribution of the two b-jet candidates before and after the jet p_T regression, for VBF signal events. The generated Higgs boson signal mass is 125 GeV and the event selection corresponds to set A. By FWHM we denote the width of the distribution at the middle of its maximum height.

7.2 Discrimination between quark- and gluon-originated jets

To further identify whether the jet pair with the smallest b-tag values among the four leading jets is likely to originate from hadronization of a light (u,d,s-type) quark, as expected for signal VBF jets, or from gluons, as is more probable for jets produced in QCD processes, a quark-gluon discriminant [43–45] is applied to the VBF candidate jets.

The discriminant exploits differences in the showering and fragmentation of gluons and quarks, making use of the following internal jet composition observables based on the PF jet constituents: (i) the major root-mean square (RMS) of the distribution of jet constituents in the $\eta\text{-}\phi$ plane [45], (ii) the minor RMS of the distribution of jet constituents in the $\eta\text{-}\phi$ plane [45], (iii) the jet asymmetry pull [46], (iv) the jet particle multiplicity, and (v) the maximum energy fraction carried by a jet constituent. The pull and RMS variables are calculated by weighting each jet constituent by its p_T squared [45].

The five variables above are used as inputs to a likelihood estimated with gluon and quark jets from simulated QCD dijet events using the TMVA package. To improve the separation power, all variables are corrected for pileup effects as a function of the FASTJET ρ density. Figure 4 shows the normalized distribution of the quark-gluon likelihood (QGL) [45] for the first VBF-

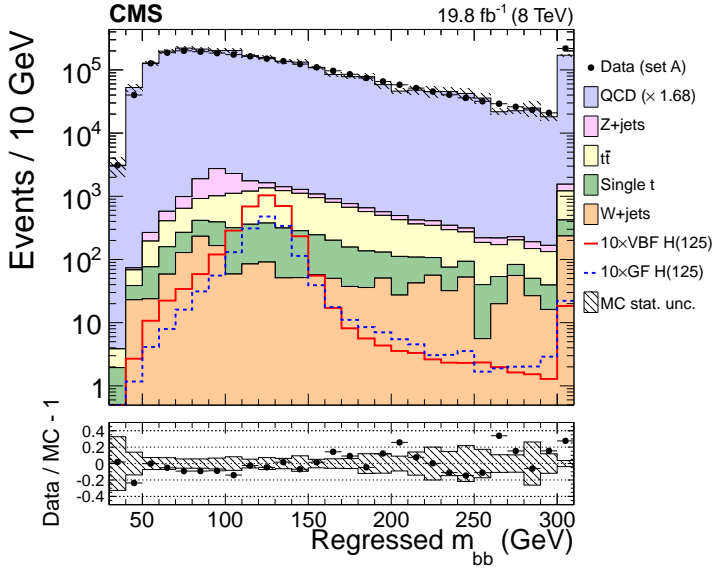


Figure 3: Distribution in invariant mass of the two b-jet candidates, after the jet p_T regression, for the events of set A. Data are shown by the points, while the simulated backgrounds are stacked. The LO QCD cross section is multiplied by a factor 1.68 so that the total number of background events equals the number of events in the data, while the VBF and GF Higgs boson signal cross sections are multiplied by a factor 10 for better visibility. The last bin is the sum of all the events beyond the range of the x axis (overflow). The panel at the bottom shows the fractional difference between the data and the background simulation, with the shaded band representing the statistical uncertainties in the MC samples.

jet candidate (the jet that is ranked third in the b-tag score; see Section 5), for background and signal events. As expected, VBF signal events, dominated by quark jets, have a pronounced peak at likelihood ~ 0 , while the background and GF events are enriched in gluon jets, and have a very different QGL distribution. The QGL distribution of all four jets is used as input to the signal vs background discriminant (Section 9.1).

7.3 Soft QCD activity

To measure the additional hadronic activity between the VBF-tagging jets, excluding the more centrally produced Higgs boson decay products, only reconstructed charged tracks are used. This is done to measure the hadronic activity associated with the primary vertex (PV), defined as the reconstructed vertex with the largest sum of squared transverse momenta of tracks used to reconstruct it.

A collection of “additional tracks” is assembled using reconstructed tracks that (i) satisfy the *high purity* quality requirements defined in Ref. [47] and $p_T > 300$ MeV; (ii) are not associated with any of the four leading PF jets in the event; (iii) have a minimum longitudinal impact parameter, $|d_z(\text{PV})|$, with respect to the main PV, rather than to other pileup interaction vertices; (iv) satisfy $|d_z(\text{PV})| < 2$ mm and $|d_z(\text{PV})| < 3\sigma_z(\text{PV})$ with respect to the PV, where $\sigma_z(\text{PV})$ is the uncertainty in $d_z(\text{PV})$; and (v) are not in the region between the two best b-tagged jets. This is defined as an ellipse in the $\eta\phi$ plane, centered on the midpoint between the two jets, with major axis of length $\Delta R(\text{bb}) + 1$, where $\Delta R(\text{bb}) = \sqrt{(\Delta\eta_{\text{bb}})^2 + (\Delta\phi_{\text{bb}})^2}$, oriented along the direction connecting the two b jets, and with minor axis of length 1.

The additional tracks are then clustered into “soft TrackJets” using the anti- k_T clustering algorithm with a distance parameter of 0.5. The use of TrackJets represents a clean and validated

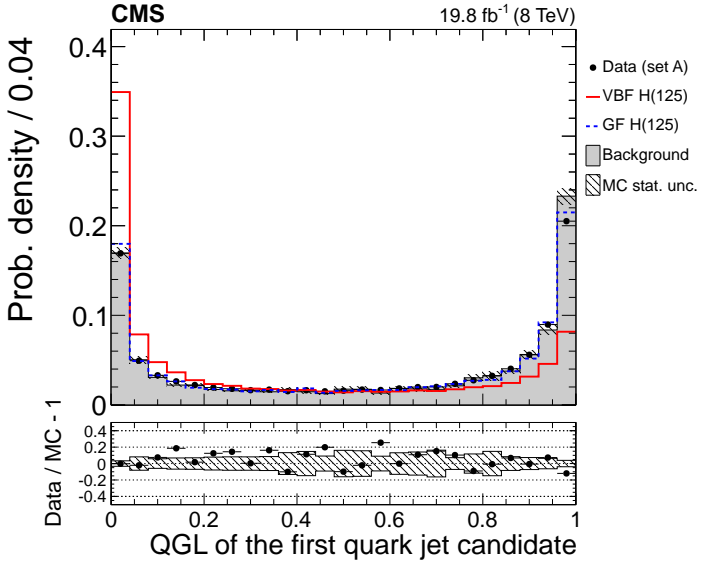


Figure 4: Normalized distribution in quark-gluon likelihood discriminant of the first light-jet candidate. Quark jets are expected to have low likelihood values (closer to 0), while gluon jets are expected to have higher ones (closer to 1). The selection corresponds to set A, data are shown by the points, and the sum of all simulated backgrounds is shown by the filled histogram. The VBF Higgs boson signal is displayed by a solid line, and the GF Higgs boson signal is shown by a dashed line. The panel at the bottom shows the fractional difference between the data and the background simulation, with the shaded band representing the statistical uncertainties in the MC samples.

method [48] to reconstruct the hadronization of partons with very low energies down to a few GeV [49]; an extensive study of the soft TrackJet activity can be found in Refs. [43, 44].

The discriminating variable, H_T^{soft} , that encapsulates the differences between the signal and the QCD background, is the scalar p_T sum of the soft TrackJets with $p_T > 1 \text{ GeV}$, and is shown in Fig. 5.

8 Extraction of the Z boson signal

The Z +jets background process, with the Z boson decaying to a b-quark pair, provides a validation of the analysis strategy used for the Higgs boson search. The extraction of the Z boson signal demonstrates the ability to observe a relatively wide hadronic resonance on top of a smooth QCD background. Also, if such a signal can be seen, it can serve for *in situ* confirmation of the scale and resolution of the invariant mass of the two b jets. Recently, the observation of a $Z \rightarrow b\bar{b}$ signal was reported by the ATLAS Collaboration [50] in the Z +1 jet final state, and similar techniques are applied here. The overall strategy has two parts. First, events are selected from set A, with the additional requirement to have at least one CSV jet. It should be noted that it is important to extract the Z boson signal in the same four-jet phase space in which the Higgs boson search is performed. Then, a multivariate discriminant is trained to separate the Z +jets process from the QCD multijet production, using variables that are only weakly correlated to m_{bb} . According to the value of the discriminant the events are divided into three categories, ranging from a signal-depleted control category, to a signal-enriched one. Finally, a simultaneous fit of the signal and the QCD background m_{bb} shape is performed in all three categories. The subsequent sections give details of the outlined procedure.

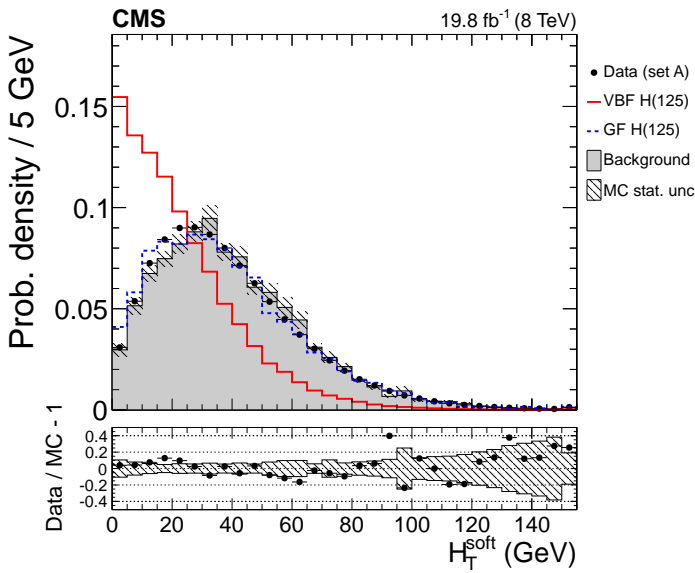


Figure 5: Normalized distribution of the scalar p_T sum of TrackJets that are associated with the soft QCD activity (H_T^{soft}). The selection corresponds to set A, data are shown by the points, and the sum of all simulated backgrounds is shown by the filled histogram. The VBF Higgs boson signal is displayed by a solid line, and the GF Higgs boson signal is shown by a dashed line. The panel at the bottom shows the fractional difference between the data and the background simulation, with the shaded band representing the statistical uncertainties in the MC samples.

8.1 Z boson signal vs. background discrimination

As discussed above, the selection of events is based on set A, with the additional requirement of having at least one CSV jet; the tightening of the b-tagging condition was found to improve the expected sensitivity. A Fisher discriminant (FD) [41] is implemented with the TMVA package and trained to discriminate between the Z + jets signal and the background. For this purpose, seven variables are used: (i) the absolute η difference $|\Delta\eta_{qq}|$ of the VBF jets; (ii) the absolute η of the b-jet system $|\eta_{bb}|$; (iii) the CSV value of the jet with highest CSV value (with best b tag); and (iv)-(vii) the QGL values of the four leading jets. Due to the very small correlations between the variables, the FD performs almost as well as more advanced, nonlinear discriminators. Figure 6 shows the normalized distribution of the discriminant, where the output of the Z + jets signal is compared to the background.

8.2 Fit of the dijet invariant mass spectrum

The selected events are divided into three categories, based on the FD output. Table 2 summarizes the event categories and corresponding yields.

Table 2: Definition of the event categories for the Z boson signal extraction and corresponding yields in the m_{bb} interval [60, 170] GeV.

	Category 1 FD < -0.02	Category 2 -0.02 < FD < 0.02	Category 3 FD > 0.02
Data	659873	374797	342931
Z + jets	1374	1467	2783
t̄t	2124	1821	2327
Single t	657	569	812

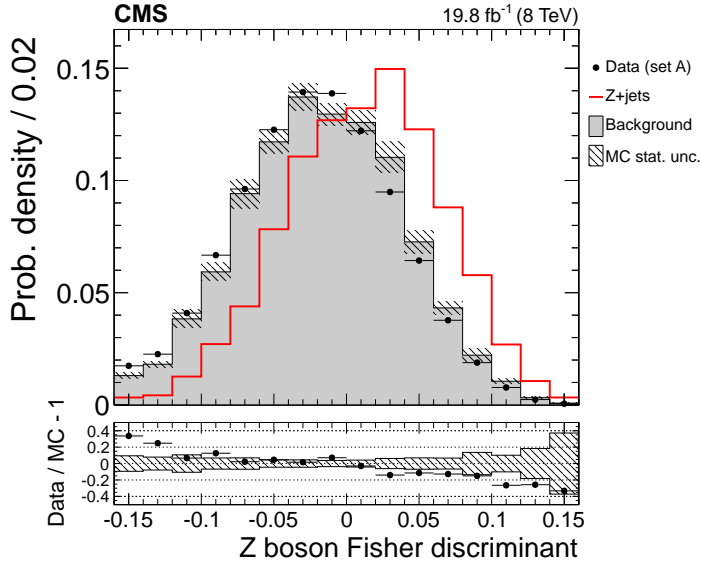


Figure 6: Normalized distribution in Z boson Fisher discriminant. Data are shown by the points, and the sum of all simulated backgrounds is shown by the filled histogram. The Z +jets signal is displayed with solid line. The panel at the bottom shows the fractional difference between the data and the background simulation, with the shaded band representing the statistical uncertainties in the MC samples.

Besides its discrimination power, the FD has minimal correlation with the invariant mass of the two b jets. This means that the m_{bb} spectrum from QCD processes is independent of the category. In practice, however, there is a small residual dependence, of up to 3%, which is corrected with a linear transfer function of m_{bb} that is taken from data. The extraction of the Z boson signal is done with a simultaneous fit in all three categories. Eq. (1) describes the fit model:

$$f_i(m_{bb}) = \mu_Z N_{i,Z} Z_i(m_{bb}; k_{\text{JES}}, k_{\text{JER}}) + N_{i,t} T_i(m_{bb}) + N_{i,\text{QCD}} K_i(m_{bb}) B8(m_{bb}; \vec{p}), \quad (1)$$

where the subscript i denotes the category, $N_{i,Z}$ is the expected yield for the Z boson signal; and μ_Z , $N_{i,\text{QCD}}$ are free parameters for the signal strength and the QCD event yield. The shape of the top quark background $T_i(m_{bb})$ is taken from the simulation (sum of the $t\bar{t}$ and single top quark contributions), and the expected yield $N_{i,t}$ is allowed to vary in the fit by 20%. The Z +jets signal shape $Z_i(m_{bb}; k_{\text{JES}}, k_{\text{JER}})$ is taken from the simulation and is parametrized as a Crystal Ball function [51] (Gaussian core with power-law tail) on top of a combinatorial background modeled by a polynomial. The position and the width of the Gaussian core are allowed to vary by the factors k_{JES} and k_{JER} , respectively, which quantify any mismatch of the jet energy scale and resolution between data and simulation and are constrained by the dedicated validation measurements of the regressed jet energy scale and resolution.

Finally, the QCD background shape in each category is described by a common, eighth-order polynomial $B8(m_{bb}; \vec{p})$, whose parameters \vec{p} are determined by the fit, and a multiplicative linear transfer function $K_i(m_{bb})$ that accounts for the small background shape differences between the categories. The choice of the polynomial is based on an extensive bias study described in Section 9. Allowing for 20% uncertainty on the Z boson signal efficiency, the simultaneous binned maximum-likelihood fit yields a signal strength of $\mu_Z = 1.10^{+0.44}_{-0.33}$, which corresponds to an observed (expected) significance of 3.6σ (3.3σ). The fitted values of k_{JES} and k_{JER} are 1.01 ± 0.02 and 1.02 ± 0.10 , respectively. Figure 7 shows the fitted distributions and the background-subtracted ones.

The extraction of the Z boson signal in this way validates the Higgs boson search method used in this paper by finding a known dijet resonance in a similar mass range. In addition, the simulated m_{bb} scale and resolution are consistent with the data, based on the best-fit values of the k_{JES} and k_{JER} nuisance parameters, which serve to constrain the corresponding uncertainties in the Higgs boson signal extraction.

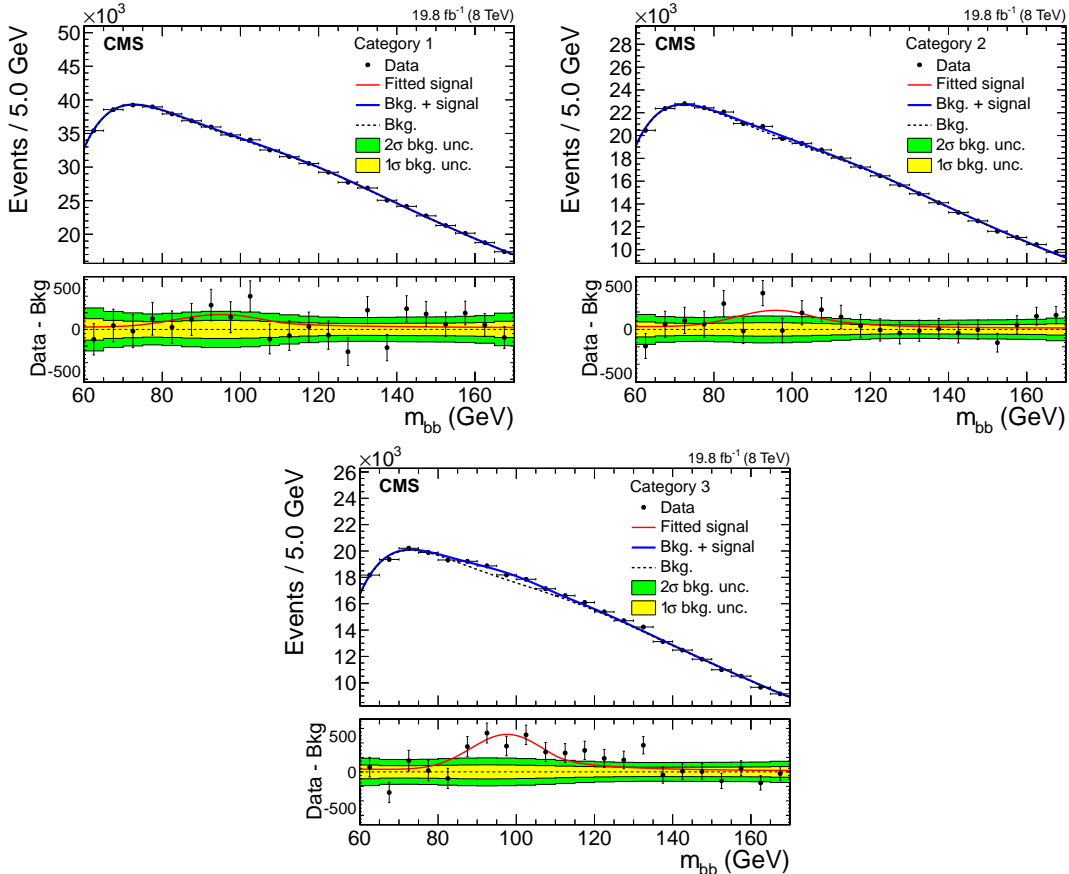


Figure 7: Invariant mass distribution of the two b-jet candidates for the Z boson signal in the three event categories that are based on the Z boson Fisher discriminant output, starting from the most backgroundlike (upper left) and ending at the most signal-like (bottom). Data are shown by the points. The solid line is the sum of the postfit background and signal shapes, while the dashed line is the background component alone. The bottom panel shows the background-subtracted distribution, overlaid with the fitted signal, and with the 1σ and 2σ background uncertainty bands. The measured (simulated) parameters of the Gaussian core of the signal shape in category 3 are 97.7(96.6) GeV and 9.3(9.1) GeV for the mean and the sigma, respectively.

9 Search for a Higgs boson

The search for a Higgs boson follows closely the methodology applied for the extraction of the Z boson signal (Section 8.2). Namely, a multivariate discriminant is employed (Section 9.1) to divide the events into seven categories that are subsequently fit simultaneously with m_{bb} templates (Section 9.2).

9.1 Higgs boson signal vs. background discrimination

In order to separate the overwhelmingly large QCD background from the Higgs boson signal, all discriminating features have to be used in an optimal way. This is best achieved by using a multivariate discriminant, which in this case is a BDT implemented with the TMVA package. The variables used as an input to the BDT are chosen such that they are very weakly correlated with the dynamics of the $b\bar{b}$ system, in particular with m_{bb} , and are grouped into five distinct groups: (i) the dynamics of the VBF-jet system, expressed by $\Delta\eta_{qq}$, $\Delta\phi_{qq}$, and m_{qq} ; (ii) the b -jet content of the event, expressed by the CSV output for the two best b -tagged jets; (iii) the jet flavor of the event QGL for all four jets; (iv) the soft activity, quantified by the scalar p_T sum H_T^{soft} of the additional soft TrackJets with $p_T > 1 \text{ GeV}$, and the number N^{soft} of soft TrackJets with $p_T > 2 \text{ GeV}$; and (v) the angular dynamics of the production mechanism, expressed by the cosine of the angle between the qq and $b\bar{b}$ planes in the center-of-mass frame of the four leading jets $\cos\theta_{qq,b\bar{b}}^*$. In practice, two BDTs are trained with the same input variables using the selections corresponding to the two sets of events. This distinction is necessary because the properties of the selected events are significantly different between the two selections (set A and set B). Figure 8 shows the output of the BDT for the two sets of events.

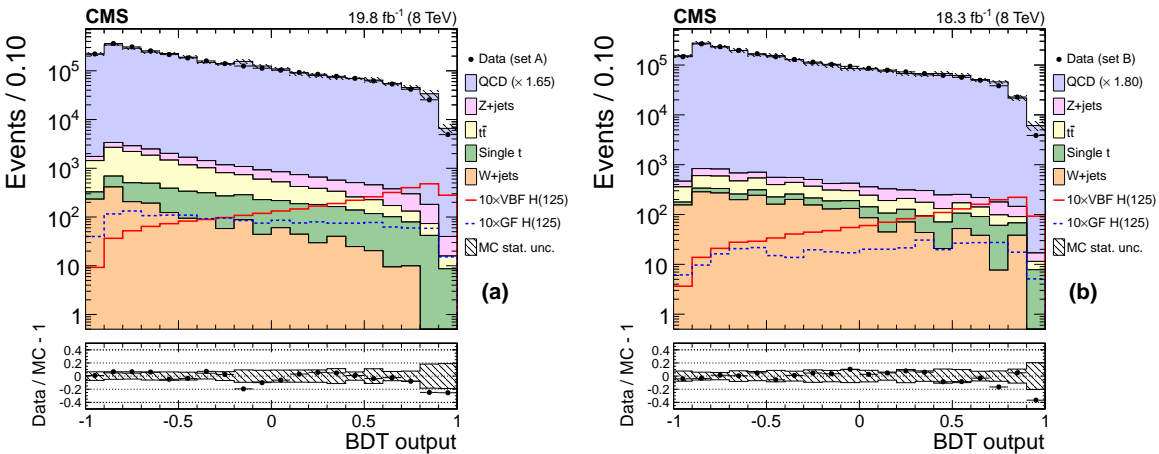


Figure 8: Distribution of the BDT output for the events of set A (a) and set B (b). Data are shown by the points, while the simulated backgrounds are stacked. The LO QCD cross sections are scaled such that the total number of background events equals the number of events in data, while the VBF and GF Higgs boson signal yields are multiplied by a factor of 10 for better visibility. The panels at the bottom show the fractional difference between the data and the background simulation, with the shaded band representing the statistical uncertainties of the MC samples.

9.2 Fit of the dijet invariant mass spectrum

Taking into account the expected sensitivity of the analysis and the available number of MC events (necessary to build the various m_{bb} templates), seven categories are defined, according to the BDT output: four for set A and three for set B. The boundaries of the categories and the respective event yields are summarized in Table 3. In an m_{bb} interval of twice the width of the Gaussian core of the signal distribution ($m_H = 125 \text{ GeV}$), the signal-over-background ratio reaches 1.7% in the most sensitive category (category 4). It should be noted that both the VBF and GF contributions are added to the Higgs boson signal, with the fraction of the latter ranging from $\sim 50\%$ in category 1 to $\sim 7\%$ in category 4.

The analysis relies on the assumption that the QCD m_{bb} spectrum shape is the same in all

Table 3: Definition of the event categories and corresponding yields in the m_{bb} interval [80, 200] GeV, for the data and the MC expectation. The BDT output boundary values refer to the distributions shown in Fig. 8.

BDT boundary values	set A				set B		
	Cat. 1	Cat. 2	Cat. 3	Cat. 4	Cat. 5	Cat. 6	Cat. 7
	-0.6 – 0.0	0.0 – 0.7	0.7 – 0.84	0.84 – 1.0	-0.1 – 0.4	0.4 – 0.8	0.8 – 1.0
Data	546121	321039	32740	10874	203865	108279	15151
Z +jets	2038	1584	198	71	435	280	45
W+jets	282	135	4	<1	225	92	17
t̄t	2818	839	45	14	342	169	21
Single t	960	633	64	25	194	159	30
VBF $m_H(125)$	53	140	58	57	33	57	31
GF $m_H(125)$	53	51	8	5	9	10	2

BDT categories of the same set of events. In reality, a small correction is needed to account for residual differences between the m_{bb} spectrum in category 1 vs. categories 2,3 and 4, and in category 5 vs. categories 6 and 7. The correction factor (transfer function) is a linear function of m_{bb} in set A and a quadratic one in set B (because a stronger dependence is observed in set B between m_{bb} and the multivariate discriminant). With the introduction of the transfer functions, the fit model for the Higgs boson signal is given by Eq. (2):

$$f_i(m_{\text{bb}}) = \mu_H N_{i,H} H_i(m_{\text{bb}}; k_{\text{JES}}, k_{\text{JER}}) + N_{i,Z} Z_i(m_{\text{bb}}; k_{\text{JES}}, k_{\text{JER}}) + N_{i,t} T_i(m_{\text{bb}}; k_{\text{JES}}, k_{\text{JER}}) + N_{i,\text{QCD}} K_i(m_{\text{bb}}) B(m_{\text{bb}}; \vec{p}_{\text{set}}), \quad (2)$$

where the subscript i denotes the category and μ_H , $N_{i,\text{QCD}}$ are free parameters for the signal strength and the QCD event yield. $N_{i,H}$, $N_{i,Z}$, and $N_{i,t}$ are the expected yields for the Higgs boson signal, the Z +jets, and the top quark background respectively. The shape of the top quark background $T_i(m_{\text{bb}}; k_{\text{JES}}, k_{\text{JER}})$ is taken from the simulation (sum of the t̄t and single top quark contributions) and is described by a broad Gaussian. The Z/W+jets background $Z_i(m_{\text{bb}}; k_{\text{JES}}, k_{\text{JER}})$ and the Higgs boson signal $H_i(m_{\text{bb}}; k_{\text{JES}}, k_{\text{JER}})$ shapes are taken from the simulation and are parametrized as a Crystal Ball function (Gaussian core with power-law tail) on top of a polynomial. The position and the width of the Gaussian core of the MC templates (signal and background) are allowed to vary by the free factors k_{JES} and k_{JER} , respectively, which quantify any mismatch of the jet energy scale and resolution between data and simulation. Finally, the QCD shape is described by a polynomial $B(m_{\text{bb}}; \vec{p}_{\text{set}})$, common within the categories of each set, and a multiplicative transfer function $K_i(m_{\text{bb}})$ per category, accounting for the shape differences between the categories. The parameters of the polynomial, \vec{p}_{set} , and those of the transfer functions, are determined by the fit, which is performed simultaneously in all categories in each set. For set A, the polynomial is of fifth order, while for set B it is of fourth order.

The choice of the QCD background shapes and event category transfer function parametrizations are fully based on data, and have been performed among classes of functions, e.g. polynomials, exponential, power laws and their combinations, with a minimum number of degrees of freedom suited to fit the data in all categories. Each function considered is used to generate different MC pseudo-data sets, and each data set is fitted using the different functional models. A potential bias on the signal estimation is computed for each pair of possible functions used to generate and fit to the pseudo-data sets. The background model chosen yields a maximum potential bias on the fitted signal strength of less than six times the statistical uncertainty on the background. Hence the systematic uncertainty associated with the background shape can be neglected.

10 Systematic uncertainties

Table 4 summarizes the sources of uncertainty related to both the background and to the signal processes. The leading uncertainty comes from the QCD background description: both the parameters of its shape and the overall normalization in each category are allowed to float freely, being determined by the simultaneous fit to the data. The resulting covariance matrix is used to compute the uncertainty. For the smaller background contributions from the Z/W+jets and top quark production, the m_{bb} shapes are taken from the simulation, while their corresponding yields are allowed to float in the fit with a 30% log-normal constraint centered on the SM expectations.

The experimental uncertainties on the jet energy scale (JES) and jet energy resolution (JER) affect the signal acceptance and the shape of the multivariate discriminant output, and are included as nuisance parameters. The effect of the JES and JER uncertainties on the m_{bb} shape is taken into account in the fit function. By varying the JES and JER by their measured uncertainties [39], the impact of the signal yield per analysis category is estimated. These variations affect the acceptance by up to 10%, while the peak position of the m_{bb} shape is shifted by 2%, and the width by 10%.

Additional uncertainties are assigned to the flavor tagging of the jets. The CSV and QGL discriminant outputs are shifted according to the observed agreement between data and simulation and the effect on the signal acceptance is estimated to range from 3% to 10% for the former, and from 1% to 3% for the latter. The impact of the CSV shift is more significant, both because it is used for the event selection, and because the multivariate discriminant depends more strongly on the b tagging of the jets. The shift of QGL only affects the shape of the discriminant, and thus the distribution of signal events in the analysis categories.

The trigger uncertainty is estimated by propagating the uncertainty in the data vs. MC simulation scale factor for the efficiency. This is achieved by convolving the two-dimensional efficiency scale factor with the signal distribution. As a result, the uncertainty in the signal yield ranges from 1% to 6% for the VBF process, and from 5% to 20% for the GF.

Theoretical uncertainties affect the signal simulation. First, the uncertainty due to PDFs and strong coupling constant α_S variation is computed to be 2.8% (VBF) and 7.5% (GF) [52]. A residual uncertainty from these sources is estimated for the particular kinematical phase space of the search: following the PDF4LHC prescription [53, 54] the PDF and α_S uncertainty ranges from 2% to 5%, while the renormalization and factorization scale variations in the signal simulation induce an uncertainty of 1% to 5% in the analysis categories, on top of a global cross section uncertainty of 0.2% (VBF) and 7.7–8.1% (GF). Finally, the variation of the UE and parton-shower (PS) model (using PYTHIA 8.1 [55] instead of the default PYTHIA 6) affects the signal acceptance by 2% to 7% (VBF) and by 10% to 45% (GF).

Lastly, an uncertainty of 2.6% is assigned to the total integrated luminosity measurement [56].

11 Results

The m_{bb} distributions in data, for all categories, are fitted simultaneously with the parametric functions described in Section 9.2 under two different hypotheses: background only and background plus a Higgs boson signal. The fit is a binned likelihood fit incorporating the systematic uncertainties discussed in Section 10 as nuisance parameters. Due to the smallness of the GF contribution in the most signal-sensitive categories we do not attempt to fit independently the VBF and the GF signal strengths. The fits in sets A and B are shown in Figs. 9 and 10, respectively. The limits on the signal strength are computed with the asymptotic CL_s

Table 4: Sources of systematic uncertainty and their impact on the shape and normalization of the background and signal processes.

Background uncertainties		
QCD shape parameters	determined by the fit	
QCD bkg. normalization	determined by the fit	
Top quark bkg. normalization	30%	
Z/W+jets bkg. normalization	30%	
Uncertainties affecting the signal		
JES (signal shape)	2%	
JER (signal shape)	10%	
Integrated luminosity	2.6%	
Branching fraction ($H \rightarrow b\bar{b}$)	2.4%–4.3%	
JES (acceptance)	6%–10%	4%–12%
JER (acceptance)	1%–4%	1%–9%
b-jet tagging	3%–9%	3%–10%
Quark/gluon-jet tagging	1%–3%	1%–3%
Trigger	1%–6%	5%–20%
Theory uncertainties		
UE & PS	2%–7%	10%–45%
Scale variation (global)	0.2%	7.7%–8.1%
Scale variation (categories)	1%–5%	1%–5%
PDF (global)	2.8%	7.5%
PDF (categories)	1.5%–3%	3.5%–5%

method [57–59]. Figure 11 shows the observed (expected) 95% confidence level (CL) limit on the total VBF plus GF signal strength, as a function of the Higgs boson mass, which ranges from 5.0 (2.2) at $m_H = 115$ GeV to 5.8 (3.7) at $m_H = 135$ GeV, together with the expected limits in the presence of a SM Higgs boson with a mass of 125 GeV. For the 125 GeV Higgs boson signal the observed (expected) significance is 2.2 (0.8) standard deviations, and the fitted signal strength is $\mu = \sigma/\sigma_{SM} = 2.8^{+1.6}_{-1.4}$. The measured signal strength is compatible with the SM Higgs boson prediction $\mu = 1$ at the 8% level.

12 Combination with other CMS Higgs boson to b-quarks searches

The CMS experiment has also performed searches for the Higgs boson decaying to bottom quarks, where the Higgs boson is produced in association with a vector boson [14] (VH), or with a top quark pair [16, 17] ($t\bar{t}H$). The VH results have been recently updated and combined with $t\bar{t}H$ [11]. Here we combine those results with the ones from the VBF production search described in this paper. Event selection overlaps between different analyses have been checked and are either empty by construction or have negligible effects on the combination. The combination methodology is based on the likelihood ratio test statistics employed in Section 11, and takes into account correlations among sources of systematic uncertainty. Care is taken to understand the behavior of the parameters that are correlated between analyses, in terms of the fitted parameter values and uncertainties.

Table 5 lists the 95% CL expected and observed upper limits and the best-fit signal strength values from the individual channels and from the combined fit. For $m_H = 125$ GeV the combination yields an $H \rightarrow b\bar{b}$ signal strength $\mu = 1.03^{+0.44}_{-0.42}$ with a significance of 2.6 standard deviations.

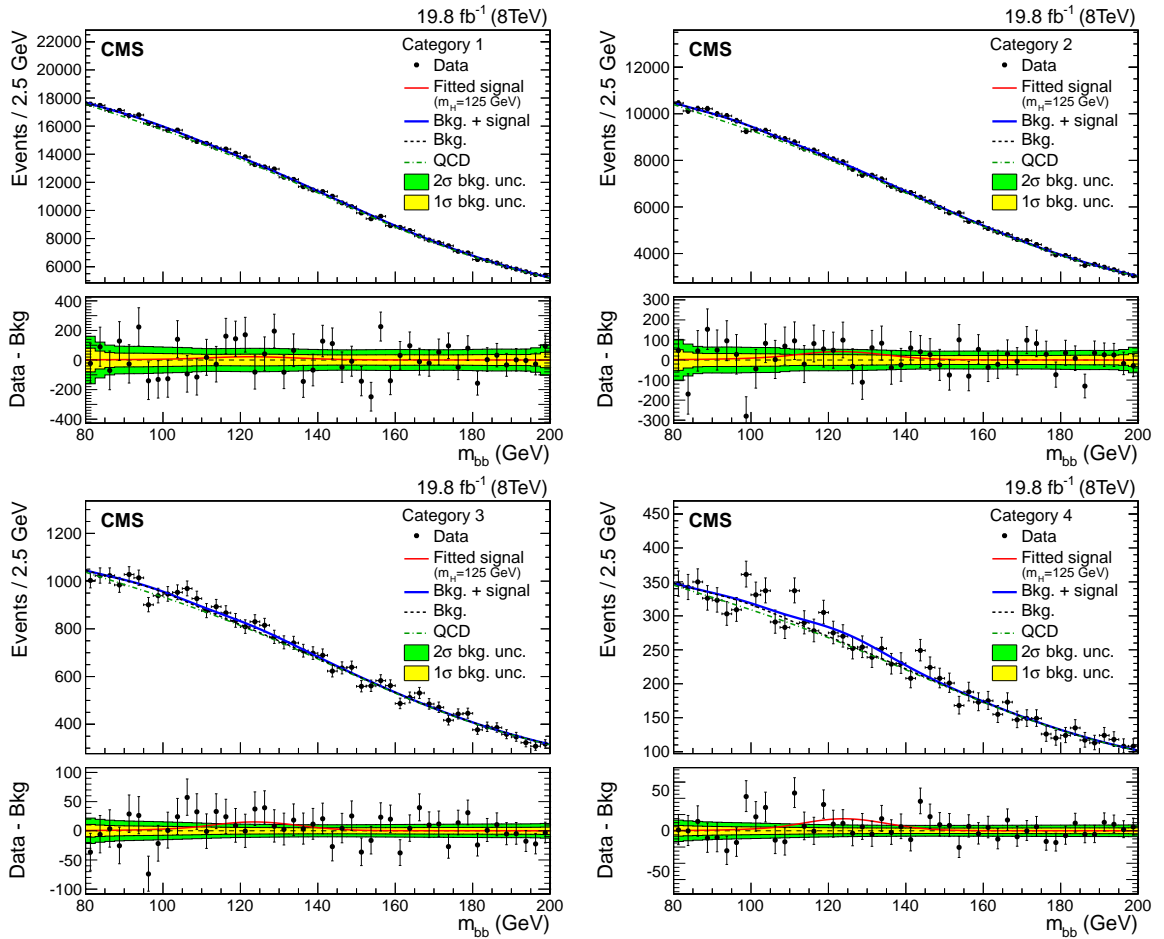


Figure 9: Fit of the invariant mass of the two b-jet candidates for the Higgs boson signal ($m_H = 125 \text{ GeV}$) in the four event categories of set A. Data are shown by the points. The solid line is the sum of the postfit background and signal shapes, the dashed line is the background component, and the dashed-dotted line is the QCD component alone. The bottom panel shows the background-subtracted distribution, overlaid with the fitted signal, and with the 1σ and 2σ background uncertainty bands.

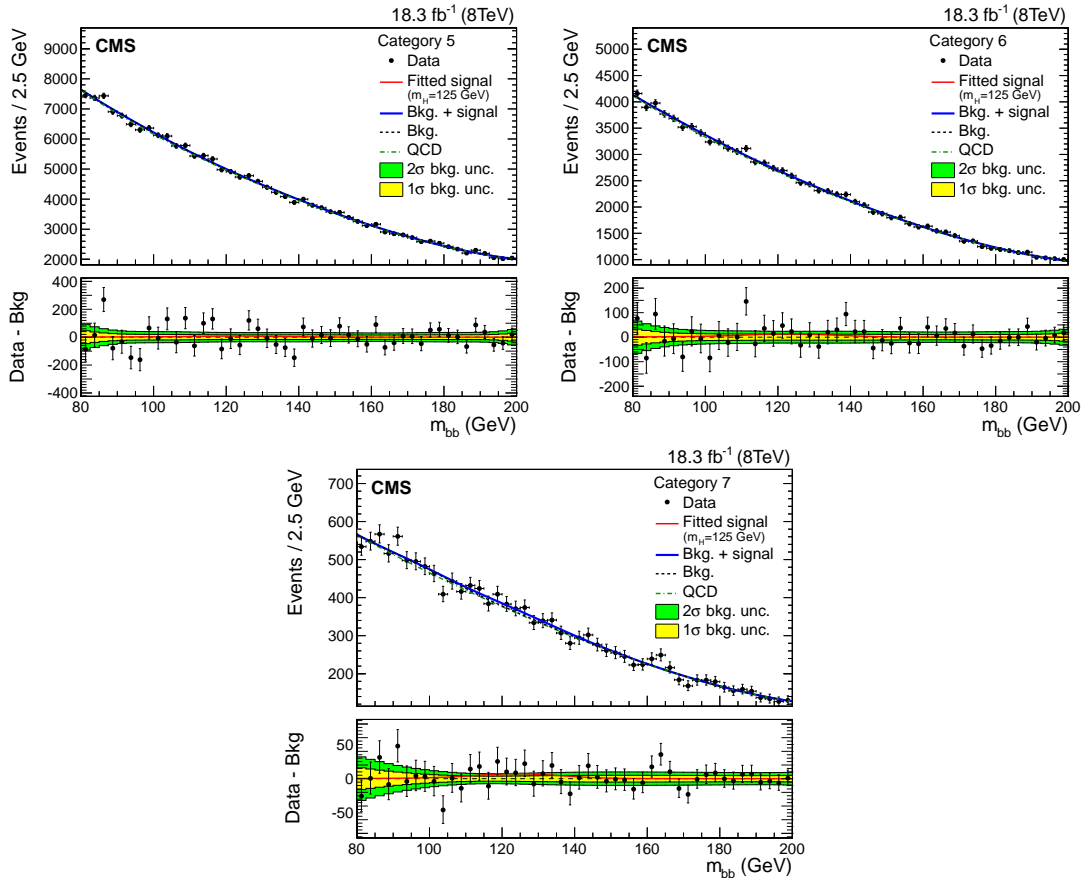


Figure 10: Fit of the invariant mass of the two b-jet candidates for the Higgs boson signal ($m_H = 125 \text{ GeV}$) in the three event categories of set B. Data are shown with markers. The solid line is the sum of the postfit background and signal shapes, the dashed line is the background component, and the dashed-dotted line is the QCD component alone. The bottom panel shows the background-subtracted distribution, overlaid with the fitted signal, and with the 1σ and 2σ background uncertainty bands.

13 Summary

A search has been carried out for the SM Higgs boson produced in vector boson fusion and decaying to $b\bar{b}$ with two data samples of pp collisions at $\sqrt{s} = 8 \text{ TeV}$ collected with the CMS detector at the LHC corresponding to integrated luminosities of 19.8 fb^{-1} and 18.3 fb^{-1} . Upper limits, at the 95% confidence level, on the production cross section times the $H \rightarrow b\bar{b}$ branching fraction, relative to expectations for a SM Higgs boson, are extracted for a Higgs boson in the mass range $115\text{--}135 \text{ GeV}$. In this range, the expected upper limits in the absence of a signal vary between a factor of 2.2 to 3.7 of the SM prediction, while the observed upper limits vary from 5.0 to 5.8. For a Higgs boson mass of 125 GeV , the observed and expected significance is, respectively, 2.2 and 0.8 standard deviations, and the fitted signal strength is $\mu = \sigma/\sigma_{\text{SM}} = 2.8^{+1.6}_{-1.4}$. This is the first search of this kind, and the only search for the SM Higgs boson in all-jet final states, at the LHC.

The combination of the results obtained in this search with other CMS $H \rightarrow b\bar{b}$ searches in the VH and $t\bar{t}H$ production modes, yields a $H \rightarrow b\bar{b}$ signal strength $\mu = 1.03^{+0.44}_{-0.42}$ with a signal significance of 2.6 standard deviations for $m_H = 125 \text{ GeV}$ that is consistent with the SM.

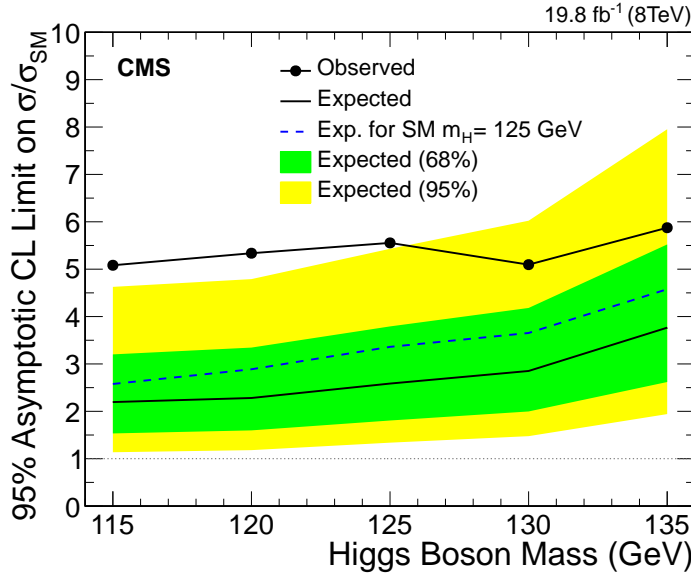


Figure 11: Expected and observed 95% confidence level limits on the signal cross section in units of the SM expected cross section, as a function of the Higgs boson mass, including all event categories. The limits expected in the presence of a SM Higgs boson with a mass of 125 GeV are indicated by the dotted curve.

Table 5: Observed and expected 95% CL limits, best fit values on the signal strength parameter $\mu = \sigma/\sigma_{\text{SM}}$ and signal significances for $m_H = 125 \text{ GeV}$, for each $H \rightarrow b\bar{b}$ channel and their combination.

$H \rightarrow b\bar{b}$ Channel	Best fit (68% CL)		Upper limits (95% CL)		Signal significance	
	Observed		Observed	Expected	Observed	Expected
VH	0.89 ± 0.43		1.68	0.85	2.08	2.52
$t\bar{t}H$	0.7 ± 1.8		4.1	3.5	0.37	0.58
VBF	$2.8^{+1.6}_{-1.4}$		5.5	2.5	2.20	0.83
Combined	$1.03^{+0.44}_{-0.42}$		1.77	0.78	2.56	2.70

Acknowledgments

We congratulate our colleagues in the CERN accelerator departments for the excellent performance of the LHC and thank the technical and administrative staffs at CERN and at other CMS institutes for their contributions to the success of the CMS effort. In addition, we gratefully acknowledge the computing centers and personnel of the Worldwide LHC Computing Grid for delivering so effectively the computing infrastructure essential to our analyses. Finally, we acknowledge the enduring support for the construction and operation of the LHC and the CMS detector provided by the following funding agencies: BMWFW and FWF (Austria); FNRS and FWO (Belgium); CNPq, CAPES, FAPERJ, and FAPESP (Brazil); MES (Bulgaria); CERN; CAS, MoST, and NSFC (China); COLCIENCIAS (Colombia); MSES and CSF (Croatia); RPF (Cyprus); MoER, ERC IUT and ERDF (Estonia); Academy of Finland, MEC, and HIP (Finland); CEA and CNRS/IN2P3 (France); BMBF, DFG, and HGF (Germany); GSRT (Greece); OTKA and NIH (Hungary); DAE and DST (India); IPM (Iran); SFI (Ireland); INFN (Italy); MSIP and NRF (Republic of Korea); LAS (Lithuania); MOE and UM (Malaysia); CINVESTAV, CONACYT, SEP, and UASLP-FAI (Mexico); MBIE (New Zealand); PAEC (Pakistan); MSHE and NSC (Poland); FCT (Portugal); JINR (Dubna); MON, RosAtom, RAS and RFBR (Russia); MESTD (Serbia); SEIDI and CPAN (Spain); Swiss Funding Agencies (Switzerland); MST (Taipei); ThEPCenter, IPST, STAR and NSTDA (Thailand); TUBITAK and TAEK (Turkey); NASU and SFFR (Ukraine); STFC (United Kingdom); DOE and NSF (USA).

Individuals have received support from the Marie-Curie program and the European Research Council and EPLANET (European Union); the Leventis Foundation; the A. P. Sloan Foundation; the Alexander von Humboldt Foundation; the Belgian Federal Science Policy Office; the Fonds pour la Formation à la Recherche dans l’Industrie et dans l’Agriculture (FRIA-Belgium); the Agentschap voor Innovatie door Wetenschap en Technologie (IWT-Belgium); the Ministry of Education, Youth and Sports (MEYS) of the Czech Republic; the Council of Science and Industrial Research, India; the HOMING PLUS program of the Foundation for Polish Science, co-financed from the European Union, Regional Development Fund; the Compagnia di San Paolo (Torino); the Consorzio per la Fisica (Trieste); MIUR project 20108T4XTM (Italy); the Thalis and Aristeia programs cofinanced by EU-ESF and the Greek NSRF; and the National Priorities Research Program by the Qatar National Research Fund.

References

- [1] A. Salam, “Weak and electromagnetic interactions”, in *Elementary particle physics: relativistic groups and analyticity*, N. Svartholm, ed., p. 367. Almqvist & Wiksell, Stockholm, 1968. Proceedings of the eighth Nobel symposium.
- [2] S. L. Glashow, “Partial-symmetries of weak interactions”, *Nucl. Phys.* **22** (1961) 579, doi:10.1016/0029-5582(61)90469-2.
- [3] S. Weinberg, “A Model of Leptons”, *Phys. Rev. Lett.* **19** (1967) 1264, doi:10.1103/PhysRevLett.19.1264.
- [4] F. Englert and R. Brout, “Broken Symmetry and the Mass of Gauge Vector Mesons”, *Phys. Rev. Lett.* **13** (1964) 321, doi:10.1103/PhysRevLett.13.321.
- [5] P. W. Higgs, “Broken Symmetries and the Masses of Gauge Bosons”, *Phys. Rev. Lett.* **13** (1964) 508, doi:10.1103/PhysRevLett.13.508.

- [6] G. S. Guralnik, C. R. Hagen, and T. W. B. Kibble, "Global Conservation Laws and Massless Particles", *Phys. Rev. Lett.* **13** (1964) 585,
[doi:10.1103/PhysRevLett.13.585](https://doi.org/10.1103/PhysRevLett.13.585).
- [7] ATLAS Collaboration, "Observation of a new particle in the search for the Standard Model Higgs boson with the ATLAS detector at the LHC", *Phys. Lett. B* **716** (2012) 1,
[doi:10.1016/j.physletb.2012.08.020](https://doi.org/10.1016/j.physletb.2012.08.020), arXiv:1207.7214.
- [8] CMS Collaboration, "Observation of a new boson at a mass of 125 GeV with the CMS experiment at the LHC", *Phys. Lett. B* **716** (2012) 30,
[doi:10.1016/j.physletb.2012.08.021](https://doi.org/10.1016/j.physletb.2012.08.021), arXiv:1207.7235.
- [9] CMS Collaboration, "Observation of a new boson with mass near 125 GeV in pp collisions at $\sqrt{s} = 7$ and 8 TeV", *JHEP* **06** (2013) 081,
[doi:10.1007/JHEP06\(2013\)081](https://doi.org/10.1007/JHEP06(2013)081), arXiv:1303.4571.
- [10] ATLAS Collaboration, "Measurements of Higgs boson production and couplings in diboson final states with the ATLAS detector at the LHC", *Phys. Lett. B* **726** (2013) 88,
[doi:10.1016/j.physletb.2013.08.010](https://doi.org/10.1016/j.physletb.2013.08.010), arXiv:1307.1427. [Erratum:
[doi:10.1016/j.physletb.2014.05.011](https://doi.org/10.1016/j.physletb.2014.05.011)].
- [11] CMS Collaboration, "Precise determination of the mass of the Higgs boson and tests of compatibility of its couplings with the standard model predictions using proton collisions at 7 and 8 TeV", *Eur. Phys. J. C* **75** (2015) 212,
[doi:10.1140/epjc/s10052-015-3351-7](https://doi.org/10.1140/epjc/s10052-015-3351-7), arXiv:1412.8662.
- [12] LHC Higgs Cross Section Working Group, S. Dittmaier et al., "Handbook of LHC Higgs Cross Sections: 2. Differential Distributions", CERN Report CERN-2012-002, 2012.
[doi:10.5170/CERN-2012-002](https://doi.org/10.5170/CERN-2012-002), arXiv:1201.3084.
- [13] CDF and D0 Collaboration, "Evidence for a Particle Produced in Association with Weak Bosons and Decaying to a Bottom-Antibottom Quark Pair in Higgs Boson Searches at the Tevatron", *Phys. Rev. Lett.* **109** (2012) 071804,
[doi:10.1103/PhysRevLett.109.071804](https://doi.org/10.1103/PhysRevLett.109.071804), arXiv:1207.6436.
- [14] CMS Collaboration, "Search for the standard model Higgs boson produced in association with W or Z bosons and decaying to bottom quarks", *Phys. Rev. D* **89** (2014) 012003,
[doi:10.1103/PhysRevD.89.012003](https://doi.org/10.1103/PhysRevD.89.012003), arXiv:1310.3687.
- [15] ATLAS Collaboration, "Search for the bbar decay of the Standard Model Higgs boson in associated (W/Z)H production with the ATLAS detector", *JHEP* **01** (2015) 069,
[doi:10.1007/JHEP01\(2015\)069](https://doi.org/10.1007/JHEP01(2015)069), arXiv:1409.6212.
- [16] CMS Collaboration, "Search for the standard model Higgs boson produced in association with a top-quark pair in pp collisions at the LHC", *JHEP* **05** (2013) 145,
[doi:10.1007/JHEP05\(2013\)145](https://doi.org/10.1007/JHEP05(2013)145), arXiv:1303.0763.
- [17] CMS Collaboration, "Search for the associated production of the Higgs boson with a top-quark pair", *JHEP* **09** (2014) 087, [doi:10.1007/JHEP09\(2014\)087](https://doi.org/10.1007/JHEP09(2014)087),
arXiv:1408.1682.
- [18] ATLAS Collaboration, "Search for the Standard Model Higgs boson produced in association with top quarks and decaying into bb̄ in pp collisions at $\sqrt{s} = 8$ TeV with the ATLAS detector", (2015). arXiv:1503.05066. Submitted to EPJC.

- [19] CDF Collaboration, “Search for the Higgs boson in the all-hadronic final state using the full CDF data set”, *JHEP* **02** (2013) 004, doi:10.1007/JHEP02(2013)004, arXiv:1208.6445.
- [20] CMS Collaboration, “The CMS experiment at the CERN LHC”, *JINST* **3** (2008) S08004, doi:10.1088/1748-0221/3/08/S08004.
- [21] P. Nason, “A New method for combining NLO QCD with shower Monte Carlo algorithms”, *JHEP* **11** (2004) 040, doi:10.1088/1126-6708/2004/11/040, arXiv:hep-ph/0409146.
- [22] P. Gononka et al., “The tauola-photos-F environment for the TAUOLA and PHOTOS packages, release II”, *Comp. Phys. Commun.* **174** (2006) 818, doi:10.1016/j.cpc.2005.12.018, arXiv:hep-ph/0312240.
- [23] T. Sjöstrand, S. Mrenna, and P. Skands, “PYTHIA 6.4 physics and manual”, *JHEP* **05** (2006) 026, doi:10.1088/1126-6708/2006/05/026, arXiv:hep-ph/0603175.
- [24] R. Field, “Early LHC Underlying Event Data - Findings and Surprises”, (2010). arXiv:1010.3558.
- [25] J. Pumplin et al., “New Generation of Parton Distributions with Uncertainties from Global QCD Analysis”, *JHEP* **07** (2012) 012, doi:10.1088/1126-6708/2002/07/012, arXiv:hep-ph/0201195.
- [26] J. Alwall et al., “MadGraph 5: going beyond”, *JHEP* **06** (2011) 128, doi:10.1007/JHEP06(2011)128, arXiv:1106.0522.
- [27] H.-L. Lai et al., “New parton distributions for collider physics”, *Phys. Rev. D* **82** (2010) 074024, doi:10.1103/PhysRevD.82.074024, arXiv:1007.2241.
- [28] R. Gavin, Y. Li, F. Petriello, and S. Quackenbush, “FEWZ 2.0: A code for hadronic Z production at next-to-next-to-leading order”, *Comput. Phys. Commun.* **182** (2011) 2388, doi:10.1016/j.cpc.2011.06.008, arXiv:1011.3540.
- [29] Y. Li and F. Petriello, “Combining QCD and electroweak corrections to dilepton production in the framework of the FEWZ simulation code”, *Phys. Rev. D* **86** (2012) 094034, doi:10.1103/PhysRevD.86.094034, arXiv:1208.5967.
- [30] R. Gavin, Y. Li, F. Petriello, and S. Quackenbush, “W physics at the LHC with FEWZ 2.1”, *Comput. Phys. Commun.* **184** (2013) 208, doi:10.1016/j.cpc.2012.09.005, arXiv:1201.5896.
- [31] M. Czakon, P. Fiedler, and A. Mitov, “Total Top-Quark Pair-Production Cross Section at Hadron Colliders Through $O(\alpha_S^4)$ ”, *Phys. Rev. Lett.* **110** (2013) 252004, doi:10.1103/PhysRevLett.110.252004, arXiv:1303.6254.
- [32] N. Kidonakis, “Differential and total cross sections for top pair and single top production”, (2012). arXiv:1205.3453.
- [33] CMS Collaboration, “Identification of b-quark jets with the CMS experiment”, *JINST* **8** (2013) P04013, doi:10.1088/1748-0221/8/04/P04013, arXiv:1211.4462.
- [34] CMS Collaboration, “Particle-flow event reconstruction in CMS and performance for jets, taus, and E_T^{miss} ”, CMS Physics Analysis Summary CMS-PAS-PFT-09-001, CERN, 2009.

- [35] CMS Collaboration, “Commissioning of the Particle-flow Event Reconstruction with the first LHC collisions recorded in the CMS detector”, CMS Physics Analysis Summary CMS-PAS-PFT-10-001, CERN, 2010.
- [36] CMS Collaboration, “Commissioning of the particle-flow reconstruction in minimum-bias and jet events from pp collisions at 7 TeV”, CMS Physics Analysis Summary CMS-PAS-PFT-10-002, CERN, 2010.
- [37] M. Cacciari and G. P. Salam, “Dispelling the N^3 myth for the k_t jet-finder”, *Phys. Lett. B* **641** (2006) 57, doi:10.1016/j.physletb.2006.08.037, arXiv:hep-ph/0512210.
- [38] M. Cacciari, G. P. Salam, and G. Soyez, “The anti- k_t jet clustering algorithm”, *JHEP* **04** (2008) 063, doi:10.1088/1126-6708/2008/04/063, arXiv:0802.1189.
- [39] CMS Collaboration, “Determination of jet energy calibration and transverse momentum resolution in CMS”, *J. Instrum.* **6** (2011) P11002, doi:10.1088/1748-0221/6/11/P11002.
- [40] CMS Collaboration, “Pileup jet identification”, CMS Physics Analysis Summary CMS-PAS-JME-13-005, CERN, 2013.
- [41] H. Voss, A. Höcker, J. Stelzer, and F. Tegenfeldt, “TMVA, the Toolkit for Multivariate Data Analysis with ROOT”, in *XIth International Workshop on Advanced Computing and Analysis Techniques in Physics Research (ACAT)*, p. 40. 2007. arXiv:physics/0703039.
- [42] M. Cacciari and G. P. Salam, “Pileup subtraction using jet areas”, *Phys. Lett. B* **659** (2008) 119, doi:10.1016/j.physletb.2007.09.077, arXiv:0707.1378.
- [43] CMS Collaboration, “Measurement of the hadronic activity in events with a Z and two jets and extraction of the cross section for the electroweak production of a Z with two jets in pp collisions at $\sqrt{s} = 7$ TeV”, *JHEP* **10** (2013) 101, doi:10.1007/JHEP10(2013)062, arXiv:1305.7389.
- [44] CMS Collaboration, “Measurement of electroweak production of two jets in association with a Z boson in proton-proton collisions at $\sqrt{s} = 8$ TeV”, *Eur. Phys. J. C* **75** (2015) 66, doi:10.1140/epjc/s10052-014-3232-5, arXiv:1410.3153.
- [45] CMS Collaboration, “Performance of quark/gluon discrimination in 8 TeV pp data”, CMS Physics Analysis Summary CMS-PAS-JME-13-002, CERN, 2013.
- [46] J. Gallicchio and M. D. Schwartz, “Seeing in Color: Jet Superstructure”, *Phys. Rev. Lett.* **105** (2010) 022001, doi:10.1103/PhysRevLett.105.022001, arXiv:1001.5027.
- [47] CMS Collaboration, “CMS tracking performance results from early LHC operation”, *Eur. Phys. J. C* **70** (2010) 1165, doi:10.1140/epjc/s10052-010-1491-3, arXiv:1007.1988.
- [48] CMS Collaboration, “Commissioning of trackjets in pp collisions at $\sqrt{s}=7$ TeV”, CMS Physics Analysis Summary CMS-PAS-JME-10-006, CERN, 2010.
- [49] CMS Collaboration, “Performance of jet reconstruction with charged tracks only”, CMS Physics Analysis Summary CMS-PAS-JME-08-001, CERN, 2009.

- [50] ATLAS Collaboration, “Measurement of the cross section of high transverse momentum $Z \rightarrow b\bar{b}$ production in proton–proton collisions at $\sqrt{s} = 8$ TeV with the ATLAS Detector”, *Phys. Lett. B* **738** (2014) 25, doi:10.1016/j.physletb.2014.09.020, arXiv:1404.7042.
- [51] M. J. Oreglia, “A study of the reactions $\psi' \rightarrow \gamma\gamma\psi$ ”. PhD thesis, Stanford University, 1980. SLAC Report SLAC-R-236, see Appendix D.
- [52] S. Heinemeyer et al., “Handbook of LHC Higgs cross sections: 3. Higgs properties”, CERN Report CERN-2013-004, 2013. doi:10.5170/CERN-2013-004, arXiv:1307.1347.
- [53] S. Alekhin et al., “The PDF4LHC Working Group Interim Report”, (2011). arXiv:1101.0536.
- [54] M. Botje et al., “The PDF4LHC Working Group Interim Recommendations”, (2011). arXiv:1101.0538.
- [55] T. Sjöstrand, S. Mrenna, and P. Skands, “A brief introduction to PYTHIA 8.1”, *Comput. Phys. Commun.* **178** (2008) 852, doi:10.1016/j.cpc.2008.01.036, arXiv:0710.3820.
- [56] CMS Collaboration, “CMS luminosity based on pixel cluster counting - summer 2013 update”, CMS Physics Analysis Summary CMS-PAS-LUM-13-001, CERN, 2013.
- [57] T. Junk, “Confidence level computation for combining searches with small statistics”, *Nucl. Instrum. Meth. A* **434** (1999) 435, doi:10.1016/S0168-9002(99)00498-2.
- [58] A. L. Read, “Presentation of search results: the CL_s technique”, *J. Phys. G* **28** (2002) 2693, doi:10.1088/0954-3899/28/10/313.
- [59] G. Cowan, K. Cranmer, E. Gross, and O. Vitells, “Asymptotic formulae for likelihood-based tests of new physics”, *Eur. Phys. J. C* **71** (2011) 1554, doi:10.1140/epjc/s10052-011-1554-0, arXiv:1007.1727.

A The CMS Collaboration

Yerevan Physics Institute, Yerevan, Armenia
V. Khachatryan, A.M. Sirunyan, A. Tumasyan

Institut für Hochenergiephysik der OeAW, Wien, Austria

W. Adam, E. Asilar, T. Bergauer, J. Brandstetter, E. Brondolin, M. Dragicevic, J. Erö, M. Flechl, M. Friedl, R. Frühwirth¹, V.M. Ghete, C. Hartl, N. Hörmann, J. Hrubec, M. Jeitler¹, V. Knünz, A. König, M. Krammer¹, I. Krätschmer, D. Liko, T. Matsushita, I. Mikulec, D. Rabady², B. Rahbaran, H. Rohringer, J. Schieck¹, R. Schöfbeck, J. Strauss, W. Treberer-Treberspurg, W. Waltenberger, C.-E. Wulz¹

National Centre for Particle and High Energy Physics, Minsk, Belarus

V. Mossolov, N. Shumeiko, J. Suarez Gonzalez

Universiteit Antwerpen, Antwerpen, Belgium

S. Alderweireldt, T. Cornelis, E.A. De Wolf, X. Janssen, A. Knutsson, J. Lauwers, S. Luyckx, S. Ochesanu, R. Rougny, M. Van De Klundert, H. Van Haevermaet, P. Van Mechelen, N. Van Remortel, A. Van Spilbeeck

Vrije Universiteit Brussel, Brussel, Belgium

S. Abu Zeid, F. Blekman, J. D'Hondt, N. Daci, I. De Bruyn, K. Deroover, N. Heracleous, J. Keaveney, S. Lowette, L. Moreels, A. Olbrechts, Q. Python, D. Strom, S. Tavernier, W. Van Doninck, P. Van Mulders, G.P. Van Onsem, I. Van Parijs

Université Libre de Bruxelles, Bruxelles, Belgium

P. Barria, C. Caillol, B. Clerbaux, G. De Lentdecker, H. Delannoy, D. Dobur, G. Fasanella, L. Favart, A.P.R. Gay, A. Grebenyuk, T. Lenzi, A. Léonard, T. Maerschalk, A. Marinov, A. Mohammadi, L. Perniè, A. Randle-conde, T. Reis, T. Seva, C. Vander Velde, P. Vanlaer, R. Yonamine, F. Zenoni, F. Zhang³

Ghent University, Ghent, Belgium

K. Beernaert, L. Benucci, A. Cimmino, S. Crucy, A. Fagot, G. Garcia, M. Gul, J. Mccartin, A.A. Ocampo Rios, D. Poyraz, D. Ryckbosch, S. Salva Diblen, M. Sigamani, N. Strobbe, M. Tytgat, W. Van Driessche, E. Yazgan, N. Zaganidis

Université Catholique de Louvain, Louvain-la-Neuve, Belgium

S. Basegmez, C. Beluffi⁴, O. Bondu, G. Bruno, R. Castello, A. Caudron, L. Ceard, G.G. Da Silveira, C. Delaere, D. Favart, L. Forthomme, A. Giannanco⁵, J. Hollar, A. Jafari, P. Jez, M. Komm, V. Lemaitre, A. Mertens, C. Nuttens, L. Perrini, A. Pin, K. Piotrzkowski, A. Popov⁶, L. Quertenmont, M. Selvaggi, M. Vidal Marono

Université de Mons, Mons, Belgium

N. Belyi, G.H. Hammad

Centro Brasileiro de Pesquisas Fisicas, Rio de Janeiro, Brazil

W.L. Aldá Júnior, G.A. Alves, L. Brito, M. Correa Martins Junior, T. Dos Reis Martins, C. Hensel, C. Mora Herrera, A. Moraes, M.E. Pol, P. Rebello Teles

Universidade do Estado do Rio de Janeiro, Rio de Janeiro, Brazil

E. Belchior Batista Das Chagas, W. Carvalho, J. Chinellato⁷, A. Custódio, E.M. Da Costa, D. De Jesus Damiao, C. De Oliveira Martins, S. Fonseca De Souza, L.M. Huertas Guativa, H. Malbouisson, D. Matos Figueiredo, L. Mundim, H. Nogima, W.L. Prado Da Silva, A. Santoro, A. Sznajder, E.J. Tonelli Manganote⁷, A. Vilela Pereira

Universidade Estadual Paulista ^a, Universidade Federal do ABC ^b, São Paulo, Brazil
 S. Ahuja^a, C.A. Bernardes^b, A. De Souza Santos^b, S. Dogra^a, T.R. Fernandez Perez Tomei^a, E.M. Gregores^b, P.G. Mercadante^b, C.S. Moon^{a,8}, S.F. Novaes^a, Sandra S. Padula^a, D. Romero Abad, J.C. Ruiz Vargas

Institute for Nuclear Research and Nuclear Energy, Sofia, Bulgaria

A. Aleksandrov, V. Genchev[†], R. Hadjiiska, P. Iaydjiev, S. Piperov, M. Rodozov, S. Stoykova, G. Sultanov, M. Vutova

University of Sofia, Sofia, Bulgaria

A. Dimitrov, I. Glushkov, L. Litov, B. Pavlov, P. Petkov

Institute of High Energy Physics, Beijing, China

M. Ahmad, J.G. Bian, G.M. Chen, H.S. Chen, M. Chen, T. Cheng, R. Du, C.H. Jiang, R. Plestina⁹, F. Romeo, S.M. Shaheen, J. Tao, C. Wang, Z. Wang, H. Zhang

State Key Laboratory of Nuclear Physics and Technology, Peking University, Beijing, China

C. Asawatangtrakuldee, Y. Ban, Q. Li, S. Liu, Y. Mao, S.J. Qian, D. Wang, Z. Xu, W. Zou

Universidad de Los Andes, Bogota, Colombia

C. Avila, A. Cabrera, L.F. Chaparro Sierra, C. Florez, J.P. Gomez, B. Gomez Moreno, J.C. Sanabria

University of Split, Faculty of Electrical Engineering, Mechanical Engineering and Naval Architecture, Split, Croatia

N. Godinovic, D. Lelas, D. Polic, I. Puljak

University of Split, Faculty of Science, Split, Croatia

Z. Antunovic, M. Kovac

Institute Rudjer Boskovic, Zagreb, Croatia

V. Brigljevic, K. Kadija, J. Luetic, L. Sudic

University of Cyprus, Nicosia, Cyprus

A. Attikis, G. Mavromanolakis, J. Mousa, C. Nicolaou, F. Ptochos, P.A. Razis, H. Rykaczewski

Charles University, Prague, Czech Republic

M. Bodlak, M. Finger¹⁰, M. Finger Jr.¹⁰

Academy of Scientific Research and Technology of the Arab Republic of Egypt, Egyptian Network of High Energy Physics, Cairo, Egypt

R. Aly, S. Aly, Y. Assran¹¹, A. Ellithi Kamel¹², A. Lotfy, M.A. Mahmoud¹³, A. Radi^{14,15}, A. Sayed^{15,14}

National Institute of Chemical Physics and Biophysics, Tallinn, Estonia

B. Calpas, M. Kadastik, M. Murumaa, M. Raidal, A. Tiko, C. Veelken

Department of Physics, University of Helsinki, Helsinki, Finland

P. Eerola, J. Pekkanen, M. Voutilainen

Helsinki Institute of Physics, Helsinki, Finland

J. Hätkönen, V. Karimäki, R. Kinnunen, T. Lampén, K. Lassila-Perini, S. Lehti, T. Lindén, P. Luukka, T. Mäenpää, T. Peltola, E. Tuominen, J. Tuominiemi, E. Tuovinen, L. Wendland

Lappeenranta University of Technology, Lappeenranta, Finland

J. Talvitie, T. Tuuva

DSM/IRFU, CEA/Saclay, Gif-sur-Yvette, France

M. Besancon, F. Couderc, M. Dejardin, D. Denegri, B. Fabbro, J.L. Faure, C. Favaro, F. Ferri, S. Ganjour, A. Givernaud, P. Gras, G. Hamel de Monchenault, P. Jarry, E. Locci, M. Machet, J. Malcles, J. Rander, A. Rosowsky, M. Titov, A. Zghiche

Laboratoire Leprince-Ringuet, Ecole Polytechnique, IN2P3-CNRS, Palaiseau, France

S. Baffioni, F. Beaudette, P. Busson, L. Cadamuro, E. Chapon, C. Charlot, T. Dahms, O. Davignon, N. Filipovic, A. Florent, R. Granier de Cassagnac, S. Lisniak, L. Mastrolorenzo, P. Miné, I.N. Naranjo, M. Nguyen, C. Ochando, G. Ortona, P. Paganini, S. Regnard, R. Salerno, J.B. Sauvan, Y. Sirois, T. Strebler, Y. Yilmaz, A. Zabi

Institut Pluridisciplinaire Hubert Curien, Université de Strasbourg, Université de Haute Alsace Mulhouse, CNRS/IN2P3, Strasbourg, France

J.-L. Agram¹⁶, J. Andrea, A. Aubin, D. Bloch, J.-M. Brom, M. Buttignol, E.C. Chabert, N. Chanon, C. Collard, E. Conte¹⁶, X. Coubez, J.-C. Fontaine¹⁶, D. Gelé, U. Goerlach, C. Goetzmann, A.-C. Le Bihan, J.A. Merlin², K. Skovpen, P. Van Hove

Centre de Calcul de l’Institut National de Physique Nucléaire et de Physique des Particules, CNRS/IN2P3, Villeurbanne, France

S. Gadrat

Université de Lyon, Université Claude Bernard Lyon 1, CNRS-IN2P3, Institut de Physique Nucléaire de Lyon, Villeurbanne, France

S. Beauceron, C. Bernet, G. Boudoul, E. Bouvier, S. Brochet, C.A. Carrillo Montoya, J. Chasserat, R. Chierici, D. Contardo, B. Courbon, P. Depasse, H. El Mamouni, J. Fan, J. Fay, S. Gascon, M. Gouzevitch, B. Ille, I.B. Laktineh, M. Lethuillier, L. Mirabito, A.L. Pequegnot, S. Perries, J.D. Ruiz Alvarez, D. Sabes, L. Sgandurra, V. Sordini, M. Vander Donckt, P. Verdier, S. Viret, H. Xiao

Institute of High Energy Physics and Informatization, Tbilisi State University, Tbilisi, Georgia

I. Bagaturia¹⁷

RWTH Aachen University, I. Physikalisches Institut, Aachen, Germany

C. Autermann, S. Beranek, M. Edelhoff, L. Feld, A. Heister, M.K. Kiesel, K. Klein, M. Lipinski, A. Ostapchuk, M. Preuten, F. Raupach, J. Sammet, S. Schael, J.F. Schulte, T. Verlage, H. Weber, B. Wittmer, V. Zhukov⁶

RWTH Aachen University, III. Physikalisches Institut A, Aachen, Germany

M. Ata, M. Brodski, E. Dietz-Laursonn, D. Duchardt, M. Endres, M. Erdmann, S. Erdweg, T. Esch, R. Fischer, A. Güth, T. Hebbeker, C. Heidemann, K. Hoepfner, D. Klingebiel, S. Knutzen, P. Kreuzer, M. Merschmeyer, A. Meyer, P. Millet, M. Olszewski, K. Padeken, P. Papacz, T. Pook, M. Radziej, H. Reithler, M. Rieger, F. Scheuch, L. Sonnenschein, D. Teyssier, S. Thüer

RWTH Aachen University, III. Physikalisches Institut B, Aachen, Germany

V. Cherepanov, Y. Erdogan, G. Flügge, H. Geenen, M. Geisler, F. Hoehle, B. Kargoll, T. Kress, Y. Kuessel, A. Künsken, J. Lingemann², A. Nehrkorn, A. Nowack, I.M. Nugent, C. Pistone, O. Pooth, A. Stahl

Deutsches Elektronen-Synchrotron, Hamburg, Germany

M. Aldaya Martin, I. Asin, N. Bartosik, O. Behnke, U. Behrens, A.J. Bell, K. Borras, A. Burgmeier, A. Cakir, L. Calligaris, A. Campbell, S. Choudhury, F. Costanza, C. Diez Pardos, G. Dolinska, S. Dooling, T. Dorland, G. Eckerlin, D. Eckstein, T. Eichhorn, G. Flucke,

E. Gallo, J. Garay Garcia, A. Geiser, A. Gzhko, P. Gunnellini, J. Hauk, M. Hempel¹⁸, H. Jung, A. Kalogeropoulos, O. Karacheban¹⁸, M. Kasemann, P. Katsas, J. Kieseler, C. Kleinwort, I. Korol, W. Lange, J. Leonard, K. Lipka, A. Lobanov, W. Lohmann¹⁸, R. Mankel, I. Marfin¹⁸, I.-A. Melzer-Pellmann, A.B. Meyer, G. Mittag, J. Mnich, A. Mussgiller, S. Naumann-Emme, A. Nayak, E. Ntomari, H. Perrey, D. Pitzl, R. Placakyte, A. Raspereza, P.M. Ribeiro Cipriano, B. Roland, M.Ö. Sahin, P. Saxena, T. Schoerner-Sadenius, M. Schröder, C. Seitz, S. Spannagel, K.D. Trippkewitz, C. Wissing

University of Hamburg, Hamburg, Germany

V. Blobel, M. Centis Vignali, A.R. Draeger, J. Erfle, E. Garutti, K. Goebel, D. Gonzalez, M. Görner, J. Haller, M. Hoffmann, R.S. Höing, A. Junkes, R. Klanner, R. Kogler, T. Lapsien, T. Lenz, I. Marchesini, D. Marconi, D. Nowatschin, J. Ott, F. Pantaleo², T. Peiffer, A. Perieanu, N. Pietsch, J. Poehlsen, D. Rathjens, C. Sander, H. Schettler, P. Schleper, E. Schlieckau, A. Schmidt, J. Schwandt, M. Seidel, V. Sola, H. Stadie, G. Steinbrück, H. Tholen, D. Troendle, E. Usai, L. Vanelderen, A. Vanhoefer

Institut für Experimentelle Kernphysik, Karlsruhe, Germany

M. Akbiyik, C. Barth, C. Baus, J. Berger, C. Böser, E. Butz, T. Chwalek, F. Colombo, W. De Boer, A. Descroix, A. Dierlamm, M. Feindt, F. Frensch, M. Giffels, A. Gilbert, F. Hartmann², U. Husemann, F. Kassel², I. Katkov⁶, A. Kornmayer², P. Lobelle Pardo, M.U. Mozer, T. Müller, Th. Müller, M. Plagge, G. Quast, K. Rabbertz, S. Röcker, F. Roscher, H.J. Simonis, F.M. Stober, R. Ulrich, J. Wagner-Kuhr, S. Wayand, T. Weiler, C. Wöhrmann, R. Wolf

Institute of Nuclear and Particle Physics (INPP), NCSR Demokritos, Aghia Paraskevi, Greece

G. Anagnostou, G. Daskalakis, T. Geralis, V.A. Giakoumopoulou, A. Kyriakis, D. Loukas, A. Markou, A. Psallidas, I. Topsis-Giotis

University of Athens, Athens, Greece

A. Agapitos, S. Kesisoglou, A. Panagiotou, N. Saoulidou, E. Tziaferi

University of Ioánnina, Ioánnina, Greece

I. Evangelou, G. Flouris, C. Foudas, P. Kokkas, N. Loukas, N. Manthos, I. Papadopoulos, E. Paradas, J. Strologas

Wigner Research Centre for Physics, Budapest, Hungary

G. Bencze, C. Hajdu, A. Hazi, P. Hidas, D. Horvath¹⁹, F. Sikler, V. Veszpremi, G. Vesztregombi²⁰, A.J. Zsigmond

Institute of Nuclear Research ATOMKI, Debrecen, Hungary

N. Beni, S. Czellar, J. Karancsi²¹, J. Molnar, Z. Szillasi

University of Debrecen, Debrecen, Hungary

M. Bartók²², A. Makovec, P. Raics, Z.L. Trocsanyi, B. Ujvari

National Institute of Science Education and Research, Bhubaneswar, India

P. Mal, K. Mandal, N. Sahoo, S.K. Swain

Panjab University, Chandigarh, India

S. Bansal, S.B. Beri, V. Bhatnagar, R. Chawla, R. Gupta, U. Bhawandeep, A.K. Kalsi, A. Kaur, M. Kaur, R. Kumar, A. Mehta, M. Mittal, N. Nishu, J.B. Singh, G. Walia

University of Delhi, Delhi, India

Ashok Kumar, Arun Kumar, A. Bhardwaj, B.C. Choudhary, R.B. Garg, A. Kumar, S. Malhotra, M. Naimuddin, K. Ranjan, R. Sharma, V. Sharma

Saha Institute of Nuclear Physics, Kolkata, India

S. Banerjee, S. Bhattacharya, K. Chatterjee, S. Dey, S. Dutta, Sa. Jain, Sh. Jain, R. Khurana, N. Majumdar, A. Modak, K. Mondal, S. Mukherjee, S. Mukhopadhyay, A. Roy, D. Roy, S. Roy Chowdhury, S. Sarkar, M. Sharan

Bhabha Atomic Research Centre, Mumbai, India

A. Abdulsalam, R. Chudasama, D. Dutta, V. Jha, V. Kumar, A.K. Mohanty², L.M. Pant, P. Shukla, A. Topkar

Tata Institute of Fundamental Research, Mumbai, India

T. Aziz, S. Banerjee, S. Bhowmik²³, R.M. Chatterjee, R.K. Dewanjee, S. Dugad, S. Ganguly, S. Ghosh, M. Guchait, A. Gurtu²⁴, G. Kole, S. Kumar, B. Mahakud, M. Maity²³, G. Majumder, K. Mazumdar, S. Mitra, G.B. Mohanty, B. Parida, T. Sarkar²³, K. Sudhakar, N. Sur, B. Sutar, N. Wickramage²⁵

Indian Institute of Science Education and Research (IISER), Pune, India

S. Sharma

Institute for Research in Fundamental Sciences (IPM), Tehran, Iran

H. Bakhshiansohi, H. Behnamian, S.M. Etesami²⁶, A. Fahim²⁷, R. Goldouzian, M. Khakzad, M. Mohammadi Najafabadi, M. Naseri, S. Pakhtinat Mehdiabadi, F. Rezaei Hosseinabadi, B. Safarzadeh²⁸, M. Zeinali

University College Dublin, Dublin, Ireland

M. Felcini, M. Grunewald

INFN Sezione di Bari ^a, Università di Bari ^b, Politecnico di Bari ^c, Bari, Italy

M. Abbrescia^{a,b}, C. Calabria^{a,b}, C. Caputo^{a,b}, S.S. Chhibra^{a,b}, A. Colaleo^a, D. Creanza^{a,c}, L. Cristella^{a,b}, N. De Filippis^{a,c}, M. De Palma^{a,b}, L. Fiore^a, G. Iaselli^{a,c}, G. Maggi^{a,c}, M. Maggi^a, G. Miniello^{a,b}, S. My^{a,c}, S. Nuzzo^{a,b}, A. Pompili^{a,b}, G. Pugliese^{a,c}, R. Radogna^{a,b}, A. Ranieri^a, G. Selvaggi^{a,b}, L. Silvestris^{a,2}, R. Venditti^{a,b}, P. Verwilligen^a

INFN Sezione di Bologna ^a, Università di Bologna ^b, Bologna, Italy

G. Abbiendi^a, C. Battilana², A.C. Benvenuti^a, D. Bonacorsi^{a,b}, S. Braibant-Giacomelli^{a,b}, L. Brigliadori^{a,b}, R. Campanini^{a,b}, P. Capiluppi^{a,b}, A. Castro^{a,b}, F.R. Cavallo^a, G. Codispoti^{a,b}, M. Cuffiani^{a,b}, G.M. Dallavalle^a, F. Fabbri^a, A. Fanfani^{a,b}, D. Fasanella^{a,b}, P. Giacomelli^a, C. Grandi^a, L. Guiducci^{a,b}, S. Marcellini^a, G. Masetti^a, A. Montanari^a, F.L. Navarria^{a,b}, A. Perrotta^a, A.M. Rossi^{a,b}, T. Rovelli^{a,b}, G.P. Siroli^{a,b}, N. Tosi^{a,b}, R. Travaglini^{a,b}

INFN Sezione di Catania ^a, Università di Catania ^b, CSFNSM ^c, Catania, Italy

G. Cappello^a, M. Chiorboli^{a,b}, S. Costa^{a,b}, F. Giordano^a, R. Potenza^{a,b}, A. Tricomi^{a,b}, C. Tuve^{a,b}

INFN Sezione di Firenze ^a, Università di Firenze ^b, Firenze, Italy

G. Barbagli^a, V. Ciulli^{a,b}, C. Civinini^a, R. D'Alessandro^{a,b}, E. Focardi^{a,b}, S. Gonzi^{a,b}, V. Gori^{a,b}, P. Lenzi^{a,b}, M. Meschini^a, S. Paoletti^a, G. Sguazzoni^a, A. Tropiano^{a,b}, L. Viliani^{a,b}

INFN Laboratori Nazionali di Frascati, Frascati, Italy

L. Benussi, S. Bianco, F. Fabbri, D. Piccolo

INFN Sezione di Genova ^a, Università di Genova ^b, Genova, Italy

V. Calvelli^{a,b}, F. Ferro^a, M. Lo Vetere^{a,b}, E. Robutti^a, S. Tosi^{a,b}

INFN Sezione di Milano-Bicocca ^a, Università di Milano-Bicocca ^b, Milano, Italy

M.E. Dinardo^{a,b}, S. Fiorendi^{a,b}, S. Gennai^a, R. Gerosa^{a,b}, A. Ghezzi^{a,b}, P. Govoni^{a,b}, S. Malvezzi^a,

R.A. Manzoni^{a,b}, B. Marzocchi^{a,b,2}, D. Menasce^a, L. Moroni^a, M. Paganoni^{a,b}, D. Pedrini^a, S. Ragazzi^{a,b}, N. Redaelli^a, T. Tabarelli de Fatis^{a,b}

INFN Sezione di Napoli ^a, **Università di Napoli 'Federico II'** ^b, **Napoli, Italy**, **Università della Basilicata** ^c, **Potenza, Italy**, **Università G. Marconi** ^d, **Roma, Italy**

S. Buontempo^a, N. Cavallo^{a,c}, S. Di Guida^{a,d,2}, M. Esposito^{a,b}, F. Fabozzi^{a,c}, A.O.M. Iorio^{a,b}, G. Lanza^a, L. Lista^a, S. Meola^{a,d,2}, M. Merola^a, P. Paolucci^{a,2}, C. Sciacca^{a,b}, F. Thyssen

INFN Sezione di Padova ^a, **Università di Padova** ^b, **Padova, Italy**, **Università di Trento** ^c, **Trento, Italy**

P. Azzi^{a,2}, N. Bacchetta^a, D. Bisello^{a,b}, A. Boletti^{a,b}, R. Carlin^{a,b}, P. Checchia^a, M. Dall'Osso^{a,b,2}, T. Dorigo^a, F. Gasparini^{a,b}, U. Gasparini^{a,b}, A. Gozzelino^a, S. Lacaprara^a, M. Margoni^{a,b}, A.T. Meneguzzo^{a,b}, F. Montecassiano^a, M. Passaseo^a, J. Pazzini^{a,b}, M. Pegoraro^a, N. Pozzobon^{a,b}, P. Ronchese^{a,b}, F. Simonetto^{a,b}, E. Torassa^a, M. Tosi^{a,b}, S. Vanini^{a,b}, M. Zanetti, P. Zotto^{a,b}, A. Zucchetta^{a,b,2}, G. Zumerle^{a,b}

INFN Sezione di Pavia ^a, **Università di Pavia** ^b, **Pavia, Italy**

A. Braghieri^a, A. Magnani^a, S.P. Ratti^{a,b}, V. Re^a, C. Riccardi^{a,b}, P. Salvini^a, I. Vai^a, P. Vitulo^{a,b}

INFN Sezione di Perugia ^a, **Università di Perugia** ^b, **Perugia, Italy**

L. Alunni Solestizi^{a,b}, M. Biasini^{a,b}, G.M. Bilei^a, D. Ciangottini^{a,b,2}, L. Fanò^{a,b}, P. Lariccia^{a,b}, G. Mantovani^{a,b}, M. Menichelli^a, A. Saha^a, A. Santocchia^{a,b}, A. Spiezzi^{a,b}

INFN Sezione di Pisa ^a, **Università di Pisa** ^b, **Scuola Normale Superiore di Pisa** ^c, **Pisa, Italy**

K. Androsov^{a,29}, P. Azzurri^a, G. Bagliesi^a, J. Bernardini^a, T. Boccali^a, G. Broccolo^{a,c}, R. Castaldi^a, M.A. Ciocci^{a,29}, R. Dell'Orso^a, S. Donato^{a,c,2}, G. Fedi, L. Foà^{a,c†}, A. Giassi^a, M.T. Grippo^{a,29}, F. Ligabue^{a,c}, T. Lomtadze^a, L. Martini^{a,b}, A. Messineo^{a,b}, F. Palla^a, A. Rizzi^{a,b}, A. Savoy-Navarro^{a,30}, A.T. Serban^a, P. Spagnolo^a, P. Squillacioti^{a,29}, R. Tenchini^a, G. Tonelli^{a,b}, A. Venturi^a, P.G. Verdini^a

INFN Sezione di Roma ^a, **Università di Roma** ^b, **Roma, Italy**

L. Barone^{a,b}, F. Cavallari^a, G. D'imperio^{a,b,2}, D. Del Re^{a,b}, M. Diemoz^a, S. Gelli^{a,b}, C. Jorda^a, E. Longo^{a,b}, F. Margaroli^{a,b}, P. Meridiani^a, F. Micheli^{a,b}, G. Organtini^{a,b}, R. Paramatti^a, F. Preiato^{a,b}, S. Rahatlou^{a,b}, C. Rovelli^a, F. Santanastasio^{a,b}, P. Traczyk^{a,b,2}

INFN Sezione di Torino ^a, **Università di Torino** ^b, **Torino, Italy**, **Università del Piemonte Orientale** ^c, **Novara, Italy**

N. Amapane^{a,b}, R. Arcidiacono^{a,c,2}, S. Argiro^{a,b}, M. Arneodo^{a,c}, R. Bellan^{a,b}, C. Biino^a, N. Cartiglia^a, M. Costa^{a,b}, R. Covarelli^{a,b}, A. Degano^{a,b}, N. Demaria^a, L. Finco^{a,b,2}, B. Kiani^{a,b}, C. Mariotti^a, S. Maselli^a, E. Migliore^{a,b}, V. Monaco^{a,b}, E. Monteil^{a,b}, M. Musich^a, M.M. Obertino^{a,b}, L. Pacher^{a,b}, N. Pastrone^a, M. Pelliccioni^a, G.L. Pinna Angioni^{a,b}, F. Ravera^{a,b}, A. Romero^{a,b}, M. Ruspa^{a,c}, R. Sacchi^{a,b}, A. Solano^{a,b}, A. Staiano^a, U. Tamponi^a

INFN Sezione di Trieste ^a, **Università di Trieste** ^b, **Trieste, Italy**

S. Belforte^a, V. Candelise^{a,b,2}, M. Casarsa^a, F. Cossutti^a, G. Della Ricca^{a,b}, B. Gobbo^a, C. La Licata^{a,b}, M. Marone^{a,b}, A. Schizzi^{a,b}, T. Umer^{a,b}, A. Zanetti^a

Kangwon National University, Chunchon, Korea

S. Chang, A. Kropivnitskaya, S.K. Nam

Kyungpook National University, Daegu, Korea

D.H. Kim, G.N. Kim, M.S. Kim, D.J. Kong, S. Lee, Y.D. Oh, A. Sakharov, D.C. Son

Chonbuk National University, Jeonju, Korea

J.A. Brochero Cifuentes, H. Kim, T.J. Kim, M.S. Ryu

Chonnam National University, Institute for Universe and Elementary Particles, Kwangju, Korea

S. Song

Korea University, Seoul, Korea

S. Choi, Y. Go, D. Gyun, B. Hong, M. Jo, H. Kim, Y. Kim, B. Lee, K. Lee, K.S. Lee, S. Lee, S.K. Park, Y. Roh

Seoul National University, Seoul, Korea

H.D. Yoo

University of Seoul, Seoul, Korea

M. Choi, H. Kim, J.H. Kim, J.S.H. Lee, I.C. Park, G. Ryu

Sungkyunkwan University, Suwon, Korea

Y. Choi, Y.K. Choi, J. Goh, D. Kim, E. Kwon, J. Lee, I. Yu

Vilnius University, Vilnius, Lithuania

A. Juodagalvis, J. Vaitkus

National Centre for Particle Physics, Universiti Malaya, Kuala Lumpur, Malaysia

I. Ahmed, Z.A. Ibrahim, J.R. Komaragiri, M.A.B. Md Ali³¹, F. Mohamad Idris³², W.A.T. Wan Abdullah

Centro de Investigacion y de Estudios Avanzados del IPN, Mexico City, Mexico

E. Casimiro Linares, H. Castilla-Valdez, E. De La Cruz-Burelo, I. Heredia-de La Cruz³³, A. Hernandez-Almada, R. Lopez-Fernandez, A. Sanchez-Hernandez

Universidad Iberoamericana, Mexico City, Mexico

S. Carrillo Moreno, F. Vazquez Valencia

Benemerita Universidad Autonoma de Puebla, Puebla, Mexico

S. Carpintero, I. Pedraza, H.A. Salazar Ibarguen

Universidad Autónoma de San Luis Potosí, San Luis Potosí, Mexico

A. Morelos Pineda

University of Auckland, Auckland, New Zealand

D. Kofcheck

University of Canterbury, Christchurch, New Zealand

P.H. Butler, S. Reucroft

National Centre for Physics, Quaid-I-Azam University, Islamabad, Pakistan

A. Ahmad, M. Ahmad, Q. Hassan, H.R. Hoorani, W.A. Khan, T. Khurshid, M. Shoaib

National Centre for Nuclear Research, Swierk, Poland

H. Bialkowska, M. Bluj, B. Boimska, T. Frueboes, M. Górska, M. Kazana, K. Nawrocki, K. Romanowska-Rybinska, M. Szleper, P. Zalewski

Institute of Experimental Physics, Faculty of Physics, University of Warsaw, Warsaw, Poland

G. Brona, K. Bunkowski, K. Doroba, A. Kalinowski, M. Konecki, J. Krolikowski, M. Misiura, M. Olszewski, M. Walczak

Laboratório de Instrumentação e Física Experimental de Partículas, Lisboa, Portugal

P. Bargassa, C. Beirão Da Cruz E Silva, A. Di Francesco, P. Faccioli, P.G. Ferreira Parracho,

M. Gallinaro, L. Lloret Iglesias, F. Nguyen, J. Rodrigues Antunes, J. Seixas, O. Toldaiev, D. Vadruccio, J. Varela, P. Vischia

Joint Institute for Nuclear Research, Dubna, Russia

S. Afanasiev, P. Bunin, M. Gavrilenco, I. Golutvin, I. Gorbunov, A. Kamenev, V. Karjavin, V. Konoplyanikov, A. Lanev, A. Malakhov, V. Matveev³⁴, P. Moisenz, V. Palichik, V. Perelygin, S. Shmatov, S. Shulha, N. Skatchkov, V. Smirnov, T. Toriashvili³⁵, A. Zarubin

Petersburg Nuclear Physics Institute, Gatchina (St. Petersburg), Russia

V. Golovtsov, Y. Ivanov, V. Kim³⁶, E. Kuznetsova, P. Levchenko, V. Murzin, V. Oreshkin, I. Smirnov, V. Sulimov, L. Uvarov, S. Vavilov, A. Vorobyev

Institute for Nuclear Research, Moscow, Russia

Yu. Andreev, A. Dermenev, S. Gninenko, N. Golubev, A. Karneyeu, M. Kirsanov, N. Krasnikov, A. Pashenkov, D. Tlisov, A. Toropin

Institute for Theoretical and Experimental Physics, Moscow, Russia

V. Epshteyn, V. Gavrilov, N. Lychkovskaya, V. Popov, I. Pozdnyakov, G. Safronov, A. Spiridonov, E. Vlasov, A. Zhokin

National Research Nuclear University 'Moscow Engineering Physics Institute' (MEPhI), Moscow, Russia

A. Bylinkin

P.N. Lebedev Physical Institute, Moscow, Russia

V. Andreev, M. Azarkin³⁷, I. Dremin³⁷, M. Kirakosyan, A. Leonidov³⁷, G. Mesyats, S.V. Rusakov, A. Vinogradov

Skobeltsyn Institute of Nuclear Physics, Lomonosov Moscow State University, Moscow, Russia

A. Baskakov, A. Belyaev, E. Boos, V. Bunichev, M. Dubinin³⁸, L. Dudko, A. Gribushin, V. Klyukhin, O. Kodolova, I. Loktin, I. Myagkov, S. Obraztsov, M. Perfilov, S. Petrushanko, V. Savrin

State Research Center of Russian Federation, Institute for High Energy Physics, Protvino, Russia

I. Azhgirey, I. Bayshev, S. Bitioukov, V. Kachanov, A. Kalinin, D. Konstantinov, V. Krychkine, V. Petrov, R. Ryutin, A. Sobol, L. Tourtchanovitch, S. Troshin, N. Tyurin, A. Uzunian, A. Volkov

University of Belgrade, Faculty of Physics and Vinca Institute of Nuclear Sciences, Belgrade, Serbia

P. Adzic³⁹, M. Ekmedzic, J. Milosevic, V. Rekovic

Centro de Investigaciones Energéticas Medioambientales y Tecnológicas (CIEMAT), Madrid, Spain

J. Alcaraz Maestre, E. Calvo, M. Cerrada, M. Chamizo Llatas, N. Colino, B. De La Cruz, A. Delgado Peris, D. Domínguez Vázquez, A. Escalante Del Valle, C. Fernandez Bedoya, J.P. Fernández Ramos, J. Flix, M.C. Fouz, P. Garcia-Abia, O. Gonzalez Lopez, S. Goy Lopez, J.M. Hernandez, M.I. Josa, E. Navarro De Martino, A. Pérez-Calero Yzquierdo, J. Puerta Pelayo, A. Quintario Olmeda, I. Redondo, L. Romero, M.S. Soares

Universidad Autónoma de Madrid, Madrid, Spain

C. Albajar, J.F. de Trocóniz, M. Missiroli, D. Moran

Universidad de Oviedo, Oviedo, Spain

H. Brun, J. Cuevas, J. Fernandez Menendez, S. Folgueras, I. Gonzalez Caballero, E. Palencia Cortezon, J.M. Vizan Garcia

Instituto de Física de Cantabria (IFCA), CSIC-Universidad de Cantabria, Santander, Spain

I.J. Cabrillo, A. Calderon, J.R. Castiñeiras De Saa, P. De Castro Manzano, J. Duarte Campderros, M. Fernandez, G. Gomez, A. Graziano, A. Lopez Virto, J. Marco, R. Marco, C. Martinez Rivero, F. Matorras, F.J. Munoz Sanchez, J. Piedra Gomez, T. Rodrigo, A.Y. Rodriguez-Marrero, A. Ruiz-Jimeno, L. Scodellaro, I. Vila, R. Vilar Cortabitarte

CERN, European Organization for Nuclear Research, Geneva, Switzerland

D. Abbaneo, E. Auffray, G. Auzinger, M. Bachtis, P. Baillon, A.H. Ball, D. Barney, A. Benaglia, J. Bendavid, L. Benhabib, J.F. Benitez, G.M. Berruti, G. Bianchi, P. Bloch, A. Bocci, A. Bonato, C. Botta, H. Breuker, T. Camporesi, G. Cerminara, S. Colafranceschi⁴⁰, M. D'Alfonso, D. d'Enterria, A. Dabrowski, V. Daponte, A. David, M. De Gruttola, F. De Guio, A. De Roeck, S. De Visscher, E. Di Marco, M. Dobson, M. Dordevic, T. du Pree, N. Dupont-Sagorin, A. Elliott-Peisert, J. Eugster, G. Franzoni, W. Funk, D. Gigi, K. Gill, D. Giordano, M. Girone, F. Glege, R. Guida, S. Gundacker, M. Guthoff, J. Hammer, M. Hansen, P. Harris, J. Hegeman, V. Innocente, P. Janot, H. Kirschenmann, M.J. Kortelainen, K. Kousouris, K. Krajczar, P. Lecoq, C. Lourenço, M.T. Lucchini, N. Magini, L. Malgeri, M. Mannelli, J. Marrouche, A. Martelli, L. Masetti, F. Meijers, S. Mersi, E. Meschi, F. Moortgat, S. Morovic, M. Mulders, M.V. Nemallapudi, H. Neugebauer, S. Orfanelli⁴¹, L. Orsini, L. Pape, E. Perez, A. Petrilli, G. Petrucciani, A. Pfeiffer, D. Piparo, A. Racz, G. Roland⁴², M. Rovere, M. Ruan, H. Sakulin, C. Schäfer, C. Schwick, A. Sharma, P. Silva, M. Simon, P. Sphicas⁴³, D. Spiga, J. Steggemann, B. Stieger, M. Stoye, Y. Takahashi, D. Treille, A. Tsirou, G.I. Veres²⁰, N. Wardle, H.K. Wöhri, A. Zagorzynska⁴⁴, W.D. Zeuner

Paul Scherrer Institut, Villigen, Switzerland

W. Bertl, K. Deiters, W. Erdmann, R. Horisberger, Q. Ingram, H.C. Kaestli, D. Kotlinski, U. Langenegger, T. Rohe

Institute for Particle Physics, ETH Zurich, Zurich, Switzerland

F. Bachmair, L. Bäni, L. Bianchini, M.A. Buchmann, B. Casal, G. Dissertori, M. Dittmar, M. Donegà, M. Dünser, P. Eller, C. Grab, C. Heidegger, D. Hits, J. Hoss, G. Kasieczka, W. Lustermann, B. Mangano, A.C. Marini, M. Marionneau, P. Martinez Ruiz del Arbol, M. Masciovecchio, D. Meister, P. Musella, F. Nessi-Tedaldi, F. Pandolfi, J. Pata, F. Pauss, L. Perrozzi, M. Peruzzi, M. Quitnat, M. Rossini, A. Starodumov⁴⁵, M. Takahashi, V.R. Tavolaro, K. Theofilatos, R. Wallny, H.A. Weber

Universität Zürich, Zurich, Switzerland

T.K. Arrestad, C. Amsler⁴⁶, L. Caminada, M.F. Canelli, V. Chiochia, A. De Cosa, C. Galloni, A. Hinzmann, T. Hreus, B. Kilminster, C. Lange, J. Ngadiuba, D. Pinna, P. Robmann, F.J. Ronga, D. Salerno, S. Taroni, Y. Yang

National Central University, Chung-Li, Taiwan

M. Cardaci, K.H. Chen, T.H. Doan, C. Ferro, M. Konyushikhin, C.M. Kuo, W. Lin, Y.J. Lu, R. Volpe, S.S. Yu

National Taiwan University (NTU), Taipei, Taiwan

P. Chang, Y.H. Chang, Y.W. Chang, Y. Chao, K.F. Chen, P.H. Chen, C. Dietz, F. Fiori, U. Grundler, W.-S. Hou, Y. Hsiung, Y.F. Liu, R.-S. Lu, M. Miñano Moya, E. Petrakou, J.f. Tsai, Y.M. Tzeng, R. Wilken

Chulalongkorn University, Faculty of Science, Department of Physics, Bangkok, Thailand
B. Asavapibhop, K. Kovitanggoon, G. Singh, N. Srimanobhas, N. Suwonjandee

Cukurova University, Adana, Turkey

A. Adiguzel, S. Cerci⁴⁷, C. Dozen, S. Girgis, G. Gokbulut, Y. Guler, E. Gurpinar, I. Hos, E.E. Kangal⁴⁸, A. Kayis Topaksu, G. Onengut⁴⁹, K. Ozdemir⁵⁰, S. Ozturk⁵¹, B. Tali⁴⁷, H. Topakli⁵¹, M. Vergili, C. Zorbilmez

Middle East Technical University, Physics Department, Ankara, Turkey

I.V. Akin, B. Bilin, S. Bilmis, B. Isildak⁵², G. Karapinar⁵³, U.E. Surat, M. Yalvac, M. Zeyrek

Bogazici University, Istanbul, Turkey

E.A. Albayrak⁵⁴, E. Gulmez, M. Kaya⁵⁵, O. Kaya⁵⁶, T. Yetkin⁵⁷

Istanbul Technical University, Istanbul, Turkey

K. Cankocak, S. Sen⁵⁸, F.I. Vardarli

Institute for Scintillation Materials of National Academy of Science of Ukraine, Kharkov, Ukraine

B. Grynyov

National Scientific Center, Kharkov Institute of Physics and Technology, Kharkov, Ukraine

L. Levchuk, P. Sorokin

University of Bristol, Bristol, United Kingdom

R. Aggleton, F. Ball, L. Beck, J.J. Brooke, E. Clement, D. Cussans, H. Flacher, J. Goldstein, M. Grimes, G.P. Heath, H.F. Heath, J. Jacob, L. Kreczko, C. Lucas, Z. Meng, D.M. Newbold⁵⁹, S. Paramesvaran, A. Poll, T. Sakuma, S. Seif El Nasr-storey, S. Senkin, D. Smith, V.J. Smith

Rutherford Appleton Laboratory, Didcot, United Kingdom

K.W. Bell, A. Belyaev⁶⁰, C. Brew, R.M. Brown, D.J.A. Cockerill, J.A. Coughlan, K. Harder, S. Harper, E. Olaiya, D. Petyt, C.H. Shepherd-Themistocleous, A. Thea, L. Thomas, I.R. Tomalin, T. Williams, W.J. Womersley, S.D. Worm

Imperial College, London, United Kingdom

M. Baber, R. Bainbridge, O. Buchmuller, A. Bundock, D. Burton, S. Casasso, M. Citron, D. Colling, L. Corpe, N. Cripps, P. Dauncey, G. Davies, A. De Wit, M. Della Negra, P. Dunne, A. Elwood, W. Ferguson, J. Fulcher, D. Futyan, G. Hall, G. Iles, G. Karapostoli, M. Kenzie, R. Lane, R. Lucas⁵⁹, L. Lyons, A.-M. Magnan, S. Malik, J. Nash, A. Nikitenko⁴⁵, J. Pela, M. Pesaresi, K. Petridis, D.M. Raymond, A. Richards, A. Rose, C. Seez, A. Tapper, K. Uchida, M. Vazquez Acosta⁶¹, T. Virdee, S.C. Zenz

Brunel University, Uxbridge, United Kingdom

J.E. Cole, P.R. Hobson, A. Khan, P. Kyberd, D. Leggat, D. Leslie, I.D. Reid, P. Symonds, L. Teodorescu, M. Turner

Baylor University, Waco, USA

A. Borzou, J. Dittmann, K. Hatakeyama, A. Kasmi, H. Liu, N. Pastika

The University of Alabama, Tuscaloosa, USA

O. Charaf, S.I. Cooper, C. Henderson, P. Rumerio

Boston University, Boston, USA

A. Avetisyan, T. Bose, C. Fantasia, D. Gastler, P. Lawson, D. Rankin, C. Richardson, J. Rohlf, J. St. John, L. Sulak, D. Zou

Brown University, Providence, USA

J. Alimena, E. Berry, S. Bhattacharya, D. Cutts, N. Dhingra, A. Ferapontov, A. Garabedian, U. Heintz, E. Laird, G. Landsberg, Z. Mao, M. Narain, S. Sagir, T. Sinthuprasith

University of California, Davis, Davis, USA

R. Breedon, G. Breto, M. Calderon De La Barca Sanchez, S. Chauhan, M. Chertok, J. Conway, R. Conway, P.T. Cox, R. Erbacher, M. Gardner, W. Ko, R. Lander, M. Mulhearn, D. Pellett, J. Pilot, F. Ricci-Tam, S. Shalhout, J. Smith, M. Squires, D. Stolp, M. Tripathi, S. Wilbur, R. Yohay

University of California, Los Angeles, USA

R. Cousins, P. Everaerts, C. Farrell, J. Hauser, M. Ignatenko, G. Rakness, D. Saltzberg, E. Takasugi, V. Valuev, M. Weber

University of California, Riverside, Riverside, USA

K. Burt, R. Clare, J. Ellison, J.W. Gary, G. Hanson, J. Heilman, M. Ivova Rikova, P. Jandir, E. Kennedy, F. Lacroix, O.R. Long, A. Luthra, M. Malberti, M. Olmedo Negrete, A. Shrinivas, H. Wei, S. Wimpenny

University of California, San Diego, La Jolla, USA

J.G. Branson, G.B. Cerati, S. Cittolin, R.T. D'Agnolo, A. Holzner, R. Kelley, D. Klein, J. Letts, I. Macneill, D. Olivito, S. Padhi, M. Pieri, M. Sani, V. Sharma, S. Simon, M. Tadel, Y. Tu, A. Vartak, S. Wasserbaech⁶², C. Welke, F. Würthwein, A. Yagil, G. Zevi Della Porta

University of California, Santa Barbara, Santa Barbara, USA

D. Barge, J. Bradmiller-Feld, C. Campagnari, A. Dishaw, V. Dutta, K. Flowers, M. Franco Sevilla, P. Geffert, C. George, F. Golf, L. Gouskos, J. Gran, J. Incandela, C. Justus, N. Mccoll, S.D. Mullin, J. Richman, D. Stuart, I. Suarez, W. To, C. West, J. Yoo

California Institute of Technology, Pasadena, USA

D. Anderson, A. Apresyan, A. Bornheim, J. Bunn, Y. Chen, J. Duarte, A. Mott, H.B. Newman, C. Pena, M. Pierini, M. Spiropulu, J.R. Vlimant, S. Xie, R.Y. Zhu

Carnegie Mellon University, Pittsburgh, USA

V. Azzolini, A. Calamba, B. Carlson, T. Ferguson, Y. Iiyama, M. Paulini, J. Russ, M. Sun, H. Vogel, I. Vorobiev

University of Colorado at Boulder, Boulder, USA

J.P. Cumalat, W.T. Ford, A. Gaz, F. Jensen, A. Johnson, M. Krohn, T. Mulholland, U. Nauenberg, J.G. Smith, K. Stenson, S.R. Wagner

Cornell University, Ithaca, USA

J. Alexander, A. Chatterjee, J. Chaves, J. Chu, S. Dittmer, N. Eggert, N. Mirman, G. Nicolas Kaufman, J.R. Patterson, A. Rinkevicius, A. Ryd, L. Skinnari, L. Soffi, W. Sun, S.M. Tan, W.D. Teo, J. Thom, J. Thompson, J. Tucker, Y. Weng, P. Wittich

Fermi National Accelerator Laboratory, Batavia, USA

S. Abdullin, M. Albrow, J. Anderson, G. Apollinari, L.A.T. Bauerdick, A. Beretvas, J. Berryhill, P.C. Bhat, G. Bolla, K. Burkett, J.N. Butler, H.W.K. Cheung, F. Chlebana, S. Cihangir, V.D. Elvira, I. Fisk, J. Freeman, E. Gottschalk, L. Gray, D. Green, S. Grünendahl, O. Gutsche, J. Hanlon, D. Hare, R.M. Harris, J. Hirschauer, B. Hooberman, Z. Hu, S. Jindariani, M. Johnson, U. Joshi, A.W. Jung, B. Klima, B. Kreis, S. Kwan[†], S. Lammel, J. Linacre, D. Lincoln, R. Lipton, T. Liu, R. Lopes De Sá, J. Lykken, K. Maeshima, J.M. Marraffino, V.I. Martinez Outschoorn, S. Maruyama, D. Mason, P. McBride, P. Merkel, K. Mishra, S. Mrenna, S. Nahm, C. Newman-Holmes, V. O'Dell, O. Prokofyev, E. Sexton-Kennedy, A. Soha, W.J. Spalding, L. Spiegel,

L. Taylor, S. Tkaczyk, N.V. Tran, L. Uplegger, E.W. Vaandering, C. Vernieri, M. Verzocchi, R. Vidal, A. Whitbeck, F. Yang, H. Yin

University of Florida, Gainesville, USA

D. Acosta, P. Avery, P. Bortignon, D. Bourilkov, A. Carnes, M. Carver, D. Curry, S. Das, G.P. Di Giovanni, R.D. Field, M. Fisher, I.K. Furic, J. Hugon, J. Konigsberg, A. Korytov, J.F. Low, P. Ma, K. Matchev, H. Mei, P. Milenovic⁶³, G. Mitselmakher, L. Muniz, D. Rank, R. Rossin, L. Shchutska, M. Snowball, D. Sperka, J. Wang, S.j. Wang, J. Yelton

Florida International University, Miami, USA

S. Hewamanage, S. Linn, P. Markowitz, G. Martinez, J.L. Rodriguez

Florida State University, Tallahassee, USA

A. Ackert, J.R. Adams, T. Adams, A. Askew, J. Bochenek, B. Diamond, J. Haas, S. Hagopian, V. Hagopian, K.F. Johnson, A. Khatiwada, H. Prosper, V. Veeraraghavan, M. Weinberg

Florida Institute of Technology, Melbourne, USA

V. Bhopatkar, M. Hohlmann, H. Kalakhety, D. Mareskas-palcek, T. Roy, F. Yumiceva

University of Illinois at Chicago (UIC), Chicago, USA

M.R. Adams, L. Apanasevich, D. Berry, R.R. Betts, I. Bucinskaite, R. Cavanaugh, O. Evdokimov, L. Gauthier, C.E. Gerber, D.J. Hofman, P. Kurt, C. O'Brien, I.D. Sandoval Gonzalez, C. Silkworth, P. Turner, N. Varelas, Z. Wu, M. Zakaria

The University of Iowa, Iowa City, USA

B. Bilki⁶⁴, W. Clarida, K. Dilisiz, S. Durgut, R.P. Gundrajula, M. Haytmyradov, V. Khristenko, J.-P. Merlo, H. Mermerkaya⁶⁵, A. Mestvirishvili, A. Moeller, J. Nachtman, H. Ogul, Y. Onel, F. Ozok⁵⁴, A. Penzo, C. Snyder, P. Tan, E. Tiras, J. Wetzel, K. Yi

Johns Hopkins University, Baltimore, USA

I. Anderson, B.A. Barnett, B. Blumenfeld, D. Fehling, L. Feng, A.V. Gritsan, P. Maksimovic, C. Martin, K. Nash, M. Osherson, M. Swartz, M. Xiao, Y. Xin

The University of Kansas, Lawrence, USA

P. Baringer, A. Bean, G. Benelli, C. Bruner, J. Gray, R.P. Kenny III, D. Majumder, M. Malek, M. Murray, D. Noonan, S. Sanders, R. Stringer, Q. Wang, J.S. Wood

Kansas State University, Manhattan, USA

I. Chakaberia, A. Ivanov, K. Kaadze, S. Khalil, M. Makouski, Y. Maravin, L.K. Saini, N. Skhirtladze, I. Svintradze, S. Toda

Lawrence Livermore National Laboratory, Livermore, USA

D. Lange, F. Rebassoo, D. Wright

University of Maryland, College Park, USA

C. Anelli, A. Baden, O. Baron, A. Belloni, B. Calvert, S.C. Eno, C. Ferraioli, J.A. Gomez, N.J. Hadley, S. Jabeen, R.G. Kellogg, T. Kolberg, J. Kunkle, Y. Lu, A.C. Mignerey, K. Pedro, Y.H. Shin, A. Skuja, M.B. Tonjes, S.C. Tonwar

Massachusetts Institute of Technology, Cambridge, USA

A. Apyan, R. Barbieri, A. Baty, K. Bierwagen, S. Brandt, W. Busza, I.A. Cali, Z. Demiragli, L. Di Matteo, G. Gomez Ceballos, M. Goncharov, D. Gulhan, G.M. Innocenti, M. Klute, D. Kovalevskyi, Y.S. Lai, Y.-J. Lee, A. Levin, P.D. Luckey, C. Mcginn, C. Mironov, X. Niu, C. Paus, D. Ralph, C. Roland, G. Roland, J. Salfeld-Nebgen, G.S.F. Stephans, K. Sumorok, M. Varma, D. Velicanu, J. Veverka, J. Wang, T.W. Wang, B. Wyslouch, M. Yang, V. Zhukova

University of Minnesota, Minneapolis, USA

B. Dahmes, A. Finkel, A. Gude, P. Hansen, S. Kalafut, S.C. Kao, K. Klapoetke, Y. Kubota, Z. Lesko, J. Mans, S. Nourbakhsh, N. Ruckstuhl, R. Rusack, N. Tambe, J. Turkewitz

University of Mississippi, Oxford, USA

J.G. Acosta, S. Oliveros

University of Nebraska-Lincoln, Lincoln, USA

E. Avdeeva, K. Bloom, S. Bose, D.R. Claes, A. Dominguez, C. Fangmeier, R. Gonzalez Suarez, R. Kamalieddin, J. Keller, D. Knowlton, I. Kravchenko, J. Lazo-Flores, F. Meier, J. Monroy, F. Ratnikov, J.E. Siado, G.R. Snow

State University of New York at Buffalo, Buffalo, USA

M. Alyari, J. Dolen, J. George, A. Godshalk, I. Iashvili, J. Kaisen, A. Kharchilava, A. Kumar, S. Rappoccio

Northeastern University, Boston, USA

G. Alverson, E. Barberis, D. Baumgartel, M. Chasco, A. Hortiangtham, A. Massironi, D.M. Morse, D. Nash, T. Orimoto, R. Teixeira De Lima, D. Trocino, R.-J. Wang, D. Wood, J. Zhang

Northwestern University, Evanston, USA

K.A. Hahn, A. Kubik, N. Mucia, N. Odell, B. Pollack, A. Pozdnyakov, M. Schmitt, S. Stoynev, K. Sung, M. Trovato, M. Velasco, S. Won

University of Notre Dame, Notre Dame, USA

A. Brinkerhoff, N. Dev, M. Hildreth, C. Jessop, D.J. Karmgard, N. Kellams, K. Lannon, S. Lynch, N. Marinelli, F. Meng, C. Mueller, Y. Musienko³⁴, T. Pearson, M. Planer, R. Ruchti, G. Smith, N. Valls, M. Wayne, M. Wolf, A. Woodard

The Ohio State University, Columbus, USA

L. Antonelli, J. Brinson, B. Bylsma, L.S. Durkin, S. Flowers, A. Hart, C. Hill, R. Hughes, K. Kotov, T.Y. Ling, B. Liu, W. Luo, D. Puigh, M. Rodenburg, B.L. Winer, H.W. Wulsin

Princeton University, Princeton, USA

O. Driga, P. Elmer, J. Hardenbrook, P. Hebda, S.A. Koay, P. Lujan, D. Marlow, T. Medvedeva, M. Mooney, J. Olsen, C. Palmer, P. Piroué, X. Quan, H. Saka, D. Stickland, C. Tully, J.S. Werner, A. Zuranski

Purdue University, West Lafayette, USA

V.E. Barnes, D. Benedetti, D. Bortoletto, L. Gutay, M.K. Jha, M. Jones, K. Jung, M. Kress, N. Leonardo, D.H. Miller, N. Neumeister, F. Primavera, B.C. Radburn-Smith, X. Shi, I. Shipsey, D. Silvers, J. Sun, A. Svyatkovskiy, F. Wang, W. Xie, L. Xu, J. Zablocki

Purdue University Calumet, Hammond, USA

N. Parashar, J. Stupak

Rice University, Houston, USA

A. Adair, B. Akgun, Z. Chen, K.M. Ecklund, F.J.M. Geurts, M. Guilbaud, W. Li, B. Michlin, M. Northup, B.P. Padley, R. Redjimi, J. Roberts, J. Rorie, Z. Tu, J. Zabel

University of Rochester, Rochester, USA

B. Betchart, A. Bodek, P. de Barbaro, R. Demina, Y. Eshaq, T. Ferbel, M. Galanti, A. Garcia-Bellido, P. Goldenzweig, J. Han, A. Harel, O. Hindrichs, A. Khukhunaishvili, G. Petrillo, M. Verzetti

The Rockefeller University, New York, USA

L. Demortier

Rutgers, The State University of New Jersey, Piscataway, USA

S. Arora, A. Barker, J.P. Chou, C. Contreras-Campana, E. Contreras-Campana, D. Duggan, D. Ferencek, Y. Gershtein, R. Gray, E. Halkiadakis, D. Hidas, E. Hughes, S. Kaplan, R. Kunnawalkam Elayavalli, A. Lath, S. Panwalkar, M. Park, S. Salur, S. Schnetzer, D. Sheffield, S. Somalwar, R. Stone, S. Thomas, P. Thomassen, M. Walker

University of Tennessee, Knoxville, USA

M. Foerster, G. Riley, K. Rose, S. Spanier, A. York

Texas A&M University, College Station, USA

O. Bouhali⁶⁶, A. Castaneda Hernandez, M. Dalchenko, M. De Mattia, A. Delgado, S. Dildick, R. Eusebi, W. Flanagan, J. Gilmore, T. Kamon⁶⁷, V. Krutelyov, R. Montalvo, R. Mueller, I. Osipenkov, Y. Pakhotin, R. Patel, A. Perloff, J. Roe, A. Rose, A. Safonov, A. Tatarinov, K.A. Ulmer²

Texas Tech University, Lubbock, USA

N. Akchurin, C. Cowden, J. Damgov, C. Dragoiu, P.R. Dudero, J. Faulkner, S. Kunori, K. Lamichhane, S.W. Lee, T. Libeiro, S. Undleeb, I. Volobouev

Vanderbilt University, Nashville, USA

E. Appelt, A.G. Delannoy, S. Greene, A. Gurrola, R. Janjam, W. Johns, C. Maguire, Y. Mao, A. Melo, P. Sheldon, B. Snook, S. Tuo, J. Velkovska, Q. Xu

University of Virginia, Charlottesville, USA

M.W. Arenton, S. Boutle, B. Cox, B. Francis, J. Goodell, R. Hirosky, A. Ledovskoy, H. Li, C. Lin, C. Neu, E. Wolfe, J. Wood, F. Xia

Wayne State University, Detroit, USA

C. Clarke, R. Harr, P.E. Karchin, C. Kottachchi Kankanamge Don, P. Lamichhane, J. Sturdy

University of Wisconsin, Madison, USA

D.A. Belknap, D. Carlsmith, M. Cepeda, A. Christian, S. Dasu, L. Dodd, S. Duric, E. Friis, B. Gomber, R. Hall-Wilton, M. Herndon, A. Hervé, P. Klabbers, A. Lanaro, A. Levine, K. Long, R. Loveless, A. Mohapatra, I. Ojalvo, T. Perry, G.A. Pierro, G. Polese, I. Ross, T. Ruggles, T. Sarangi, A. Savin, A. Sharma, N. Smith, W.H. Smith, D. Taylor, N. Woods

†: Deceased

1: Also at Vienna University of Technology, Vienna, Austria

2: Also at CERN, European Organization for Nuclear Research, Geneva, Switzerland

3: Also at State Key Laboratory of Nuclear Physics and Technology, Peking University, Beijing, China

4: Also at Institut Pluridisciplinaire Hubert Curien, Université de Strasbourg, Université de Haute Alsace Mulhouse, CNRS/IN2P3, Strasbourg, France

5: Also at National Institute of Chemical Physics and Biophysics, Tallinn, Estonia

6: Also at Skobeltsyn Institute of Nuclear Physics, Lomonosov Moscow State University, Moscow, Russia

7: Also at Universidade Estadual de Campinas, Campinas, Brazil

8: Also at Centre National de la Recherche Scientifique (CNRS) - IN2P3, Paris, France

9: Also at Laboratoire Leprince-Ringuet, Ecole Polytechnique, IN2P3-CNRS, Palaiseau, France

10: Also at Joint Institute for Nuclear Research, Dubna, Russia

11: Also at Suez University, Suez, Egypt

-
- 12: Also at Cairo University, Cairo, Egypt
 - 13: Also at Fayoum University, El-Fayoum, Egypt
 - 14: Also at British University in Egypt, Cairo, Egypt
 - 15: Now at Ain Shams University, Cairo, Egypt
 - 16: Also at Université de Haute Alsace, Mulhouse, France
 - 17: Also at Ilia State University, Tbilisi, Georgia
 - 18: Also at Brandenburg University of Technology, Cottbus, Germany
 - 19: Also at Institute of Nuclear Research ATOMKI, Debrecen, Hungary
 - 20: Also at Eötvös Loránd University, Budapest, Hungary
 - 21: Also at University of Debrecen, Debrecen, Hungary
 - 22: Also at Wigner Research Centre for Physics, Budapest, Hungary
 - 23: Also at University of Visva-Bharati, Santiniketan, India
 - 24: Now at King Abdulaziz University, Jeddah, Saudi Arabia
 - 25: Also at University of Ruhuna, Matara, Sri Lanka
 - 26: Also at Isfahan University of Technology, Isfahan, Iran
 - 27: Also at University of Tehran, Department of Engineering Science, Tehran, Iran
 - 28: Also at Plasma Physics Research Center, Science and Research Branch, Islamic Azad University, Tehran, Iran
 - 29: Also at Università degli Studi di Siena, Siena, Italy
 - 30: Also at Purdue University, West Lafayette, USA
 - 31: Also at International Islamic University of Malaysia, Kuala Lumpur, Malaysia
 - 32: Also at Malaysian Nuclear Agency, MOSTI, Kajang, Malaysia
 - 33: Also at CONSEJO NATIONAL DE CIENCIA Y TECNOLOGIA, MEXICO, Mexico
 - 34: Also at Institute for Nuclear Research, Moscow, Russia
 - 35: Also at Institute of High Energy Physics and Informatization, Tbilisi State University, Tbilisi, Georgia
 - 36: Also at St. Petersburg State Polytechnical University, St. Petersburg, Russia
 - 37: Also at National Research Nuclear University 'Moscow Engineering Physics Institute' (MEPhI), Moscow, Russia
 - 38: Also at California Institute of Technology, Pasadena, USA
 - 39: Also at Faculty of Physics, University of Belgrade, Belgrade, Serbia
 - 40: Also at Facoltà Ingegneria, Università di Roma, Roma, Italy
 - 41: Also at National Technical University of Athens, Athens, Greece
 - 42: Also at Scuola Normale e Sezione dell'INFN, Pisa, Italy
 - 43: Also at University of Athens, Athens, Greece
 - 44: Also at Warsaw University of Technology, Institute of Electronic Systems, Warsaw, Poland
 - 45: Also at Institute for Theoretical and Experimental Physics, Moscow, Russia
 - 46: Also at Albert Einstein Center for Fundamental Physics, Bern, Switzerland
 - 47: Also at Adiyaman University, Adiyaman, Turkey
 - 48: Also at Mersin University, Mersin, Turkey
 - 49: Also at Cag University, Mersin, Turkey
 - 50: Also at Piri Reis University, Istanbul, Turkey
 - 51: Also at Gaziosmanpasa University, Tokat, Turkey
 - 52: Also at Ozyegin University, Istanbul, Turkey
 - 53: Also at Izmir Institute of Technology, Izmir, Turkey
 - 54: Also at Mimar Sinan University, Istanbul, Istanbul, Turkey
 - 55: Also at Marmara University, Istanbul, Turkey
 - 56: Also at Kafkas University, Kars, Turkey
 - 57: Also at Yildiz Technical University, Istanbul, Turkey

- 58: Also at Hacettepe University, Ankara, Turkey
- 59: Also at Rutherford Appleton Laboratory, Didcot, United Kingdom
- 60: Also at School of Physics and Astronomy, University of Southampton, Southampton, United Kingdom
- 61: Also at Instituto de Astrofísica de Canarias, La Laguna, Spain
- 62: Also at Utah Valley University, Orem, USA
- 63: Also at University of Belgrade, Faculty of Physics and Vinca Institute of Nuclear Sciences, Belgrade, Serbia
- 64: Also at Argonne National Laboratory, Argonne, USA
- 65: Also at Erzincan University, Erzincan, Turkey
- 66: Also at Texas A&M University at Qatar, Doha, Qatar
- 67: Also at Kyungpook National University, Daegu, Korea